violet was extracted from the stained cells with 2% sodium dodecyl sulfate, and the intensities were quantified spectrophotometrically 620 nm. The percent cell viability was calculated by comparison with the absorbance of control cells.

Statistical analyses

Data are expressed as mean ± SD of triplicate determinations. Comparison of 2 groups was made with an unpaired, two-tailed student's *t*-test. Comparison of multiple groups was made with ANOVA followed by Dunnett or Tukey test. A value of $p < 0.05$ was considered statistically significant.

Results

A miR-125b complementary sequence on the 3′-UTR of human VDR mRNA

By a computational search (http://www.targetscan.org/), several miRNAs are found to share complementarity with a sequence in the 3′-UTR of human VDR mRNA. Among them, we focused on miR-125b because its binding site is highly conserved among species (Fig. 1). The seed sequence of miR-125b was perfectly matching with the predicted binding site of the VDR mRNA. We investigated whether miR-125b might be involved in the regulation of human VDR expression through the MRE125b.

Expression levels of miR-125b in human cancer cell lines

For gain- and loss-of-function experiments, we need to know the expression level of endogenous miR-125b in cell lines. For this purpose, the expression levels of mature miR-125b in 6 kinds of human cancer cell lines were determined by real-time RT-PCR analysis. As shown in Figure 2*a*, the mature miR-125b level was highest in KGN followed by MDA-MB-435 cells, whereas it was extremely low in MCF-7, HepG2, HEK293 and LS180 cells.

Effects of overexpression or inhibition of miR-125b on luciferase activity

To investigate whether MRE125b is functional in the regulation by miR-125b, luciferase assays were performed. First, we transfected the precursor for miR-125b into MCF-7 cells in which the mature miR-125b level was low (Fig. 2*b*). Using the pGL3/c-125b plasmid containing the miR-125b complementary sequence, it was demonstrated that the luciferase activity was significantly ($p < 0.001$) decreased by the transfection of precursor for miR-125b. The luciferase activity of the pGL3/F1 plasmid was significantly ($p < 0.001$) decreased (60% of control) by the overexpression of miR-125b, but that of the pGL3/R1 plasmid was not. When the pGL3/3xMRE plasmid containing 3 copies of the MRE125b was used, a prominent suppression was observed (40% of control, $p < 0.001$) by the overexpression of miR-125b. Next, we transfected the AsO for miR-125b into KGN cells in which the mature miR-125b was highly expressed (Fig. 2*b*). The luciferase activity of the pGL3/c-125b plasmid was significantly ($p < 0.01$) lower than that of the control pGL3-p plasmid. The luciferase activity of the pGL3/c-125b plasmid was significantly ($p < 0.01$) restored by the transfection of AsO for miR-125b (3.1-fold of control). The luciferase activity of the pGL3/F1 plasmid was increased by the transfection of AsO for miR-125b, although the effects were statistically insignificant. The luciferase activity of the pGL3/3xMRE plasmid was significantly ($p < 0.01$) lower than that of the control pGL3-p plasmid. The luciferase activity of the pGL3/3xMRE plasmid was significantly (1.3-fold of control, $p < 0.05$) restored by the inhibition of miR-125b by AsO. These results suggest that miR-125b functionally recognized the MRE125b on the human VDR mRNA.

Effects of overexpression of miR-125b on the endogenous VDR protein level

We sought to examine the effects of miR-125b on the endogenous VDR protein level. When we first attempted to determine the endogenous VDR protein level in human cancer cell lines by Western blot analysis using commercially available antibodies, we could not identify the VDR protein because of multiple nonspecific bands. Therefore, we utilized electrophoretic mobility shift assays to evaluate the endogenous VDR level. The VDRE of human *CYP24* gene, which is known to be a target of VDR,[18] was used as a probe. It was confirmed that *in vitro*-synthesized VDR/RXRα heterodimers bound to the VDRE (Fig. 3*a*). With the anti-VDR or anti-RXRα antibodies, the band density of the VDR/RXRα heterodimer was decreased and the supershifted band was observed. When the probe was incubated with the nuclear extracts prepared from MCF-7 cells, the band representing the VDR/RXRα heterodimer was observed and the band density was diminished with the anti-VDR or anti-RXRα antibodies. When the precursor for miR-125b was transfected, the mature miR-125b level was prominently increased, and the band density of the VDR/RXRα heterodimer was significantly ($p < 0.001$) decreased compared with that of control (40% of control). We confirmed by Western blot analysis that the expression level of RXRα was not affected by the overexpression of miR-125b (data not shown). These results suggest that the endogenous VDR level was repressed by miR-125b.

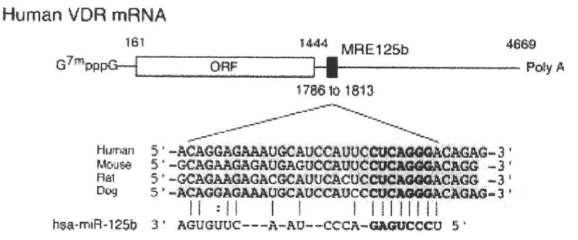

FIGURE 1 – Schematic representation of human VDR mRNA and the predicted target sequence of miR-125b. The numbering refers to the 5′ end of mRNA as 1, and the coding region is from +161 to +1444. MRE125b is located on +1786 to +1813 in the 3′-UTR of human VDR mRNA. Gray box, highly conserved regions; bold letters, seed sequence.

MiR-125b-dependent VDR regulation affects the target gene expression

We investigated whether the miR-125b-dependent regulation of VDR affects the expression of target genes. When the MCF-7 cells were treated with 100 nM $1,25(OH)_2D_3$, the CYP24 mRNA level was significantly ($p < 0.001$) increased (588-fold) (Fig. 4). However, this induction was markedly attenuated by the overexpression of miR-125b. In addition, the basal CYP24 mRNA level was also decreased by the overexpression of miR-125b, although it was statistically insignificant. These results support that the endogenous VDR level was repressed by miR-125b, and this regulation mechanism affects the expression of target genes.

Effects of overexpression of miR-125b on the antiproliferative effects of $1,25(OH)_2D_3$

We investigated the effects of miR-125b on the antiproliferative effects of $1,25(OH)_2D_3$ (Fig. 5). The cells transfected with the precursor for control were grown during incubation for 48–96 hr, but the growth was significantly ($p < 0.01$ or $p < 0.001$) reduced in the presence of 1 μM $1,25(OH)_2D_3$. Interestingly, the overexpression of miR-125b prominently ($p < 0.05$, $p < 0.01$ or $p < 0.001$) abolished the antiproliferative effects of $1,25(OH)_2D_3$. In addition, the overexpression of miR-125b could significantly ($p < 0.05$, at 96 hr) increase the cell growth in the absence of $1,25(OH)_2D_3$. These results suggest that miR-125b regulating VDR has a great impact on antiproliferative effects of $1,25(OH)_2D_3$.

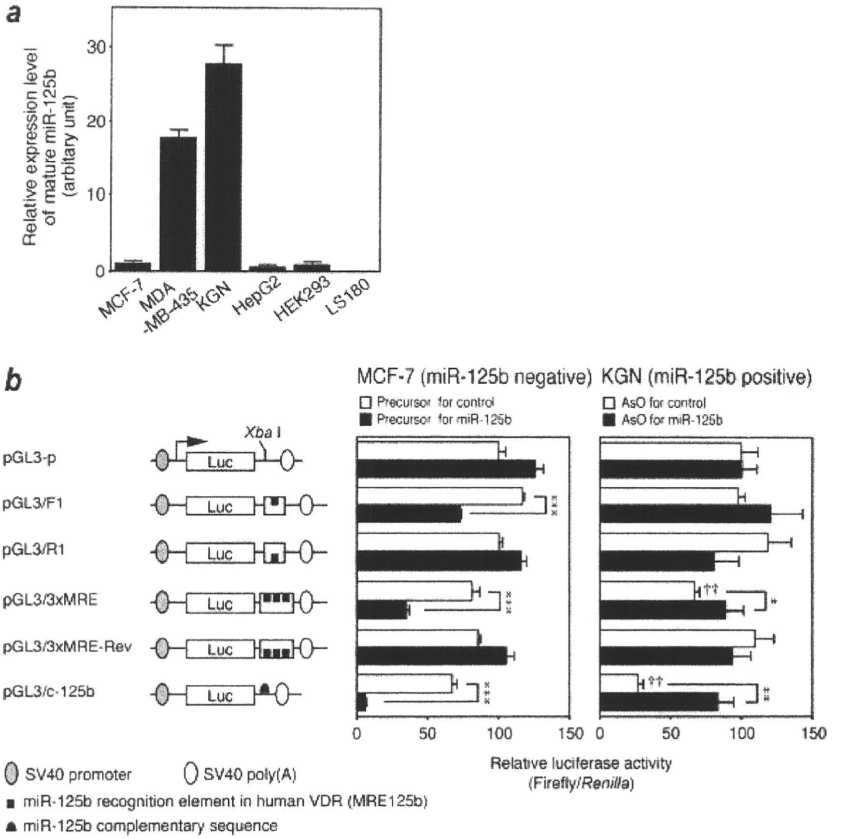

FIGURE 2 – Expression levels of mature miR-125b in various human cell lines and luciferase assays in MCF-7 and KGN cells. (*a*) The expression levels of mature miR-125b in MCF-7, MDA-MB-435, KGN, HepG2, HEK293 and LS180 cells were determined by real-time RT-PCR analysis using an NCode miRNA first-strand cDNA synthesis kit. The values were the mature miR-125b levels relative to those in MCF-7 cells. (*b*) Luciferase assays were performed to investigate whether MRE125b is functional in the regulation by miR-125b. A series of reporter constructs was transiently transfected with 10 pmol precursors for miR-125b or control into 5×10^4 MCF-7 cells, or with 5 pmol AsO for miR-125b or control into 8×10^4 KGN cells. The firefly luciferase activity for each construct was normalized with the *Renilla* luciferase activities. Values are expressed as percentages of the relative luciferase activity of pGL3-promoter plasmid. Each column represents the mean ± SD of 3 independent experiments. $*p < 0.05$, $**p < 0.01$, $***p < 0.001$, compared with the precursor or AsO for control. $\dagger\dagger p < 0.01$, compared with pGL3-p.

Discussion

In this study, we investigated whether human VDR might be regulated by miRNA. In the 3′-UTR of human VDR mRNA, a potential miR-125b recognition element (MRE125b) was identified. Luciferase assays clearly revealed that the miR-125b negatively regulated the reporter activity through MRE125b. By electrophoretic mobility shift assays and evaluation of the induction potencies of CYP24 mRNA, it was demonstrated that the endogenous VDR level was repressed by the overexpression of miR-125b. These results clearly suggest that the human VDR is post-transcriptionally regulated by miR-125b. Because the sequences of VDR mRNA around MRE125b are highly conserved among species (Fig. 1), the regulation by miR-125b may also occur in other species.

The global expression of miRNAs is deregulated in most cancer types.[21] Some studies have suggested that miRNA expression would be widely downregulated in human tumors relative to normal tissues, and other studies reported a tumor-specific mixed pattern of downregulation and upregulation of miRNA genes. Recent findings revealed that the miRNA deregulation in human cancers occurs by multiple mechanisms, including transcriptional deregulation, epigenetic alterations, mutation, DNA copy number abnormalities and dysfunction of key proteins in the miRNA biogenesis pathway.[21] Among them, alterations in DNA copy numbers would be a major mechanism because over 50% of miRNAs are in genomic fragile sites or regions associated with cancers.[12] It has been reported that miR-125b was downregulated in breast[12,22] and prostate[23] cancers. Mature miR-125b is formed by 2 precursors, miR-125b-1 and miR-125b-2. The genes for miR-125b-1 and miR-125b-2 are located in chromosome 11q24.1 and 21q11.2, respectively (http://microrna.sanger.ac.uk/sequences/). Interestingly, it has been reported that the chromosome region 11q23-24 is most frequently deleted in breast, ovarian and lung cancers[24,25] and the chromosome region 21q11-21 is frequently deleted in breast, esophagus, stomach, ovary and lung cancers.[26] This could be one of the mechanisms of the downregulation of miR-125b in cancers. Meanwhile, it is known that VDR is upregulated in several cancers,[8,9] and the upregulation appears to be associated with a good prognosis.[27] As this study demonstrated that miR-125b negatively regulated the expression of VDR, it was directly proven that the upregulation of VDR in cancers would be due to the downregulation of miR-125b.

Previously, the role of miR-125b in cell proliferation and differentiation has been reported in human prostate cancer cell lines,[28] thyroid carcinoma cells,[29] a bone marrow stroma cell line[30] and

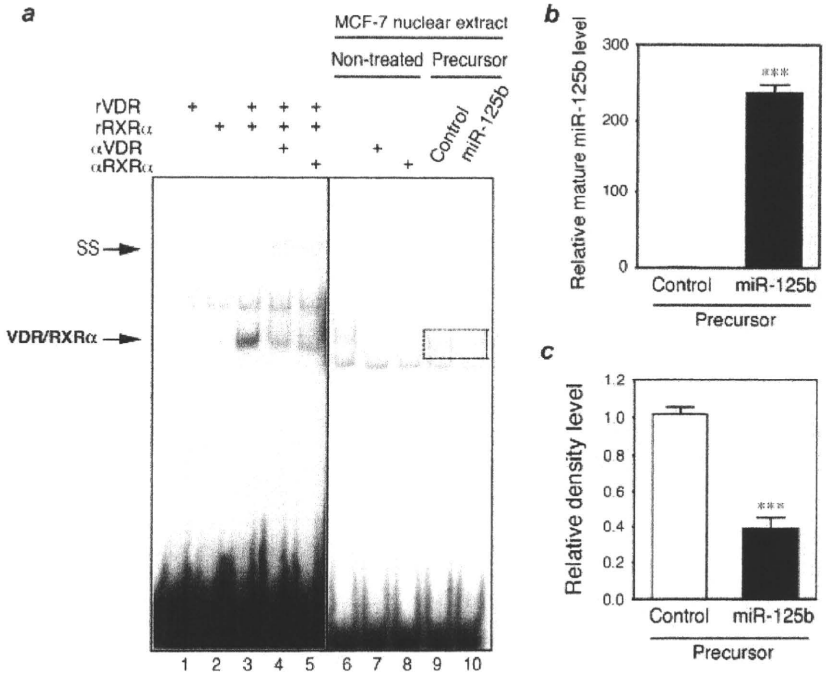

FIGURE 3 – Electrophoretic mobility shift assays to evaluate the endogenous VDR protein level. (*a*) Electrophoretic mobility shift assays were performed with oligonucleotide probe containing the VDRE in the human CYP24 promoter. The ^{32}P labeled probe was incubated with *in vitro*-synthesized VDR (rVDR) and RXRα (rRXRα) or the nuclear extract prepared from the precursors for miR-125b or control-transfected MCF-7 cells. For supershift analysis, 0.2 μg of anti-VDR antibodies (αVDR) or 2 μg of anti-RXRα antibodies (αRXRα) were preincubated with *in vitro*-synthesized proteins or the nuclear extract at room temperature for 30 min. The lower arrow indicates the VDR/RXRα-dependent shifted band and the upper arrow indicates the supershifted (SS) complex. (*b*) The mature miR-125b level was determined by real-time RT-PCR analysis. Total RNA was prepared from MCF-7 cells 72 hr after the transfection of the precursors for miR-125b or control (50 nM). The values are the mature miR-125b levels normalized with the U6 snRNA levels relative to control. (*c*) The relative density of the shifted band including VDR/RXRα complex. Each column represents the mean ± SD of 3 independent experiments. $***p < 0.001$, compared with the precursor for control.

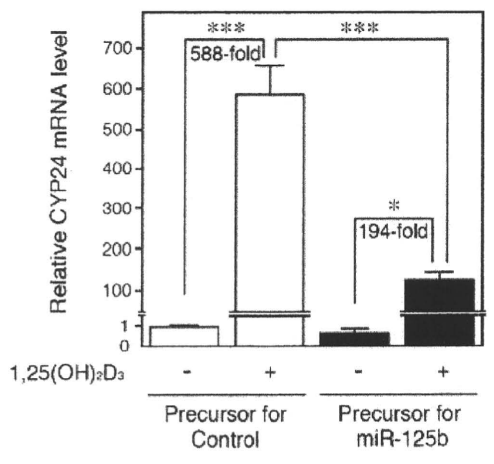

FIGURE 4 – Induction of CYP24 mRNA in MCF-7 cells by $1,25(OH)_2D_3$. The precursors for miR-125b or control (50 nM) were transfected into MCF-7 cells. After 72 hr, the cells were treated with 100 nM $1,25(OH)_2D_3$ or 0.1% ethanol (vehicle) for 24 hr and then total RNA was prepared. The CYP24 mRNA levels were determined by real-time RT-PCR and normalized with the GAPDH mRNA level. The data are expressed relative to the CYP24 mRNA level in the precursor for control-transfected cells in the absence of $1,25(OH)_2D_3$. Each column represents the mean ± SD of 3 independent experiments. $*p < 0.05$; $***p < 0.001$.

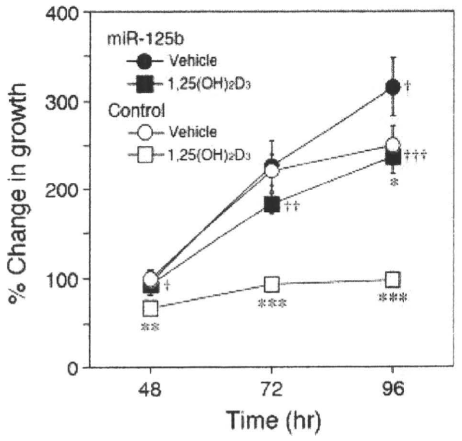

FIGURE 5 – Antiproliferative effects of $1,25(OH)_2D_3$ in MCF-7 cells. The precursors for miR-125b or control (20 nM) were transfected into MCF-7 cells. After 24 hr, the cells were treated with 1 μM $1,25(OH)_2D_3$ or 0.1% ethanol (vehicle) for 48–96 hr and then crystal violet assays were performed. Values are expressed as percentages change in growth relative to the cell viability in the precursor for control-transfected cells in the absence of $1,25(OH)_2D_3$ after 48 hr incubation. Each point represents the mean ± SD of 3 independent experiments. $*p < 0.05$, $**p < 0.01$, $***p < 0.001$, compared with the vehicle. $\dagger p < 0.05$, $\dagger\dagger p < 0.01$, $\dagger\dagger\dagger p < 0.001$, compared with the precursor for control.

hepatocellular carcinoma.[31] Scott *et al.*[32] reported that the miR-125b suppressed *ERBB2* and *ERBB3* oncogenes. Li *et al.*[31] reported that high expression of miR-125b was correlated with good survival in hepatocellular carcinoma patients. These previous studies suggest that miR-125b acts as a type of tumor suppressor gene. In contrast, our study demonstrated that miR-125b repressed the antiproliferative effects of $1,25(OH)_2D_3$. Thus, this study provides new information concerning the role of miR-125b in cell proliferation. In cancer cells, the downregulation of miR-125b would result in an augmentation of the antitumor effects of $1,25(OH)_2D_3$.

As regards other nuclear receptors, there are a few reports. Estrogen receptor (ER) α, which is an important marker for the prognosis and is predictive of the response to endocrine therapy in breast cancer patients, has been found to be regulated by miR-206[33] and miR-221/222.[34] These studies suggested that these miRNAs could serve as potential therapeutic targets for a subset of ERα-negative breast cancers. Previously, we found that pregnane X receptor (PXR), which is a key regulator of the expression of drug-metabolizing enzymes and transporters involved in the responses to steroids and xenobiotics, is regulated by miR-148a.[35] Thus, accumulating evidence has revealed that nuclear receptors, to which steroid hormones bind as a ligand, are regulated by miRNAs. The regulation of nuclear receptors by miRNA would result in changes in the expression of a variety of target genes, constructing complex regulatory networks.

In conclusion, we clarified that human VDR is posttranscriptionally regulated by miR-125b. This study could provide new insights into the regulatory mechanism of VDR expression.

Acknowledgements

The authors acknowledge Mr. Brent Bell for reviewing the manuscript.

References

1. Dusso AS, Brown AJ, Slatopolsky E. Vitamin D. Am J Physiol Renal Physiol 2005;289:F8–F28.
2. Nagpal S, Na S, Rathnachalam R. Noncalcemic actions of vitamin D receptor ligands. Endocr Rev 2005;26:662–87.
3. Holick MF. Vitamin D deficiency. N Engl J Med 2007;357:266–81.
4. Garland CF, Garland FC, Gorham ED, Lipkin M, Newmark H, Mohr SB, Holick MF. The role of vitamin D in cancer prevention. Am J Public Health 2006;96:252–61.
5. Carlberg C, Polly P. Gene regulation by vitamin D_3. Crit Rev Eukaryot Gene Expr 1998;8:19–42.
6. Zou A, Elgort MG, Allegretto EA. Retinoid X receptor (RXR) ligands activate the human 25-hydroxyvitamin D_3-24-hydroxylase promoter via RXR heterodimer binding to two vitamin D-responsive elements and elicit additive effects with 1,25-dihydroxyvitamin D_3. J Biol Chem 1997;272:19027–34.
7. Segura C, Alonso M, Fraga C, García-Caballero T, Diéguez C, Pérez-Fernández R. Vitamin D receptor ontogenesis in rat liver. Histochem Cell Biol 1999;112:163–7.
8. Friedrich M, Axt-Fliedner R, Villena-Heinsen C, Tilgen W, Schmidt W, Reichrath J. Analysis of vitamin D-receptor (VDR) and retinoid X-receptor α in breast cancer. Histochem J 2002;34:35–40.
9. Khadzkou K, Buchwald P, Westin G, Dralle H, Akerström G, Hellman P. 25-Hydroxyvitamin D_3 1α-hydroxylase and vitamin D receptor expression in papillary thyroid carcinoma. J Histochem Cytochem 2006;54:355–61.
10. Cross HS, Bareis P, Hofer H, Bischof MG, Bajna E, Kriwanek S, Bonner E, Peterlik M. 25-Hydroxyvitamin D_3-1α-hydroxylase and vitamin D receptor gene expression in human colonic mucosa is elevated during early cancerogenesis. Steroids 2001;66:287–92.
11. Ambros V. The functions of animal microRNAs. Nature 2004; 431:350–5.
12. Calin GA, Sevignani C, Dumitru CD, Hyslop T, Noch E, Yendamuri S, Shimizu M, Rattan S, Bullrich F, Negrini M, Croce CM. Human microRNA genes are frequently located at fragile sites and genomic regions involved in cancers. Proc Natl Acad Sci USA 2004; 101:2999–3004.
13. Lu J, Getz G, Miska EA, Alvarez-Saavedra E, Lamb J, Peck D, Sweet-Cordero A, Ebert BL, Mark RH, Ferrando AA, Downing JR, Jacks T, et al. MicroRNA expression profiles classify human cancers. Nature 2005;435:834–8.
14. Bartel DP. MicroRNAs: genomics, biogenesis, mechanism, and function. Cell 2004;116:281–97.
15. Lewis BP, Burge CB, Bartel DP. Conserved seed pairing, often flanked by adenosines, indicates that thousands of human genes are microRNA targets. Cell 2005;120:15–20.
16. Nishi Y, Yanase T, Mu YM, Oba K, Ichino I, Saito M, Nomura M, Mukasa C, Okabe T, Goto K, Takayanagi R, Kashimura Y, et al. Establishment and characterization of a steroidogenic human granulosa-like tumor cell line. KGN, that expresses functional follicle-stimulating hormone receptor. Endocrinology 2001;142:437–45.
17. Itoh M, Nakajima M, Higashi E, Yoshida R, Nagata K, Yamazoe Y, Yokoi T. Induction of human CYP2A6 is mediated by the pregnane X receptor with peroxisome proliferator-activated receptor-γ coactivator 1α. J Pharmacol Exp Ther 2006;319:693–702.
18. Chen KS, DeLuca HF. Cloning of the human 1α,25-dihydroxyvitamin D-3 24-hydroxylase gene promoter and identification of two vitamin D-responsive elements. Biochim Biophys Acta 1995;1263:1–9.
19. Tsuchiya Y, Nakajima M, Kyo S, Kanaya T, Inoue M, Yokoi T. Human CYP1B1 is regulated by estradiol via estrogen receptor. Cancer Res 2004;64:3119–25.
20. McGaffin KR, Acktinson LE, Chrysogelos SA. Growth and EGFR regulation in breast cancer cells by vitamin D and retinoid compounds. Breast Cancer Res Treat 2004;86:55–73.
21. Deng S, Calin GA, Croce CM, Coukos G, Zhang L. Mechanisms of microRNA deregulation in human cancer. Cell Cycle 2008;7:2643–6.
22. Iorio MV, Ferracin M, Liu CG, Veronese A, Spizzo R, Sabbioni S, Magri E, Pedriali M, Fabbri M, Campiglio M, Menard S, Palazzo JP, et al. MicroRNA gene expression deregulation in human breast cancer. Cancer Res 2005;65:7065–70.
23. Ozen M, Creighton CJ, Ozdemir M, Ittmann M. Widespread deregulation of microRNA expression in human prostate cancer. Oncogene 2007;27:1788–93.
24. Negrini M, Rasio D, Hampton GM, Sabbioni S, Rattan S, Carter SL, Rosenberg AL, Schwartz GF, Shiloh Y, Cavenee WK, Croce CM. Definition and refinement of chromosome 11 regions of loss of heterozygosity in breast cancer: identification of a new region at 11q23.3. Cancer Res 1995;55:3003–7.
25. Rasio D, Negrini M, Manenti G, Dragani TA, Croce CM. Loss of heterozygosity at chromosome 11q in lung adenocarcinoma: identification of three independent regions. Cancer Res 1995;55:3988–91.
26. Yamada H, Yanagisawa K, Tokumaru S, Taguchi A, Nimura Y, Osada H, Nagino M, Takahashi T. Detailed characterization of a homozygously deleted region corresponding to a candidate tumor suppressor locus at 21q11-21 in human lung cancer. Genes Chromosomes Cancer 2008;47:810–18.
27. Seubwai W, Wongkham C, Puapairoj A, Khuntikeo N, Wongkham S. Overexpression of vitamin D receptor indicates a good prognosis for cholangiocarcinoma: implications for therapeutics. Cancer 2007;109: 2497–505.
28. Lee YS, Kim HK, Chung S, Kim K-S, Dutta A. Depletion of human micro-RNA miR-125b reveals that it is critical for the proliferation of differentiated cells but not for the down-regulation of putative targets during differentiation. J Biol Chem 2005;280:16635–41.
29. Visone R, Pallante P, Vecchione A, Cirombella R, Ferracin M, Ferraro A, Volinica S, Coluzzi S, Leone V, Borbone E, Liu C-G, Petrocca F, et al. Specific microRNAs are downregulated in human thyroid anaplastic carcinomas. Oncogene 2007;26:7590–5.
30. Mizuno Y, Yagi K, Tokuzawa Y, Kanesaki-Yatsuka Y, Suda T, Katagiri T, Fukuda T, Maruyama M, Okuda A, Amemiya T, Kondoh Y, Tashiro H, et al. MiR-125b inhibits osteoblastic differentiation by down-regulation of cell proliferation. Biochem Biophys Res Commun 2008;368:267–72.
31. Li W, Xie L, He X, Li J, Tu K, Wei L, Wu J, Guo Y, Ma X, Zhang P, Pan Z, Hu X, et al. Diagnostic and prognostic implications of microRNAs in human hepatocellular carcinoma. Int J Cancer 2008;123: 1616–22.
32. Scott GK, Goga A, Berger C, Sullivan CS, Benz CC. Coordinate suppression of ERBB2 and ERBB3 by enforced expression of microRNA miR-125a or miR-125b. J Biol Chem 2007;282:1479–86.
33. Adams BD, Furneaux H, White BA. The micro-ribonucleic acid (miRNA) miR-206 targets the human estrogen receptor-α (ERα) and represses ERα messenger RNA and protein expression in breast cancer cell lines. Mol Endocrinol 2007;21:1132–47.
34. Zhao JJ, Lin J, Yang H, Kong W, He L, Ma X, Coppola D, Cheng JQ. MicroRNA-221/222 negatively regulates ERα and associates with tamoxifen resistance in breast cancer. J Biol Chem 2008;283:31079–86.
35. Takagi S, Nakajima M, Mohri T, Yokoi T. Post-transcriptional regulation of human pregnane X receptor by micro-RNA affects the expression of cytochrome P450 3A4. J Biol Chem 2008;283:9674–80.

Toxicology 264 (2009) 89–95

Contents lists available at ScienceDirect

Toxicology

journal homepage: www.elsevier.com/locate/toxicol

Knockdown of superoxide dismutase 2 enhances acetaminophen-induced hepatotoxicity in rat

Yukitaka Yoshikawa[a], Mayu Morita[a], Hiroko Hosomi[a], Koichi Tsuneyama[b], Tatsuki Fukami[a], Miki Nakajima[a], Tsuyoshi Yokoi[a,*]

[a] Drug Metabolism and Toxicology, Faculty of Pharmaceutical Sciences, Kanazawa University, Kakuma-machi, Kanazawa 920-1192, Japan
[b] Department of Diagnostic Pathology, Graduate School of Medicine and Pharmaceutical Science for Research, University of Toyama, Sugitani, Toyama 930-0194, Japan

ARTICLE INFO

Article history:
Received 29 May 2009
Received in revised form 22 July 2009
Accepted 23 July 2009
Available online 30 July 2009

Keywords:
Superoxide dismutase 2
Acetaminophen
RNA interference
Hepatotoxicity

ABSTRACT

Drug-induced hepatotoxicity is a major problem in drug development, and oxidative stress is known as one of the causes. Superoxide dismutases (SODs) are important antioxidant enzymes against reactive oxygen species (ROS). Mitochondria are the major source of superoxide production, and SOD2 is mainly localized in mitochondria and, with other SODs, plays an important role in scavenging superoxide. Previously, we reported the establishment of an adenovirus vector with short hairpin RNA against rat SOD2 (AdSOD2-shRNA), and applied this to evaluate drug-induced cytotoxicity. In this study, infection of AdSOD2-shRNA to Fisher 344 rats resulted in a significant decrease of SOD2 mRNA, protein expression, and SOD2 enzyme activity to 28%, 35%, and 39%, respectively, 7 days after infection. Serum AST and ALT were significantly increased by single oral administration of acetaminophen (1000 mg/kg) to these SOD2-knockdown rats without fasting compared with the control adenovirus infected groups. Heme oxygenase-1 protein, known to be induced by oxidative stress, was detected in SOD2-knockdown rats administered acetaminophen. In addition, protein carbonyl and lipid peroxidation, also known to be induced by oxidative stress, were significantly increased in SOD2 knockdown rats. This is the first report of a SOD2-knockdown rat model that could be useful to evaluate the drug-induced hepatotoxicity with high sensitivity.

1. Introduction

Oxidative stress is one of the causes of drug-induced hepatotoxicity (Kaplowitz, 2005) and is known to be induced by superoxide, which is mainly generated in mitochondria. Superoxide is able to react with NO to form peroxynitrite or, after conversion to hydrogenperoxide, undergo metal-catalysed Fenton reactions to form highly reactive hydroxyl radicals (Boelsterli and Lim, 2006). Superoxide dismutases (SODs) are the first and most important line of antioxidant enzymes against reactive oxygen species (ROS) and, particularly, superoxide anion radicals (Zelko et al., 2002). At present, three distinct SOD isoforms, SOD1, SOD2, and SOD3, have been identified in mammals. SOD1, SOD2 and SOD3 are mainly localized to the cytoplasm, mitochondria and plasma, respectively (Zelko et al., 2002). In addition, SOD2 is known to be induced by a wide range of compounds, including anticancer drugs and lipopolysaccharide (Das et al., 1998; Visner et al., 1990). Meanwhile, the importance of the SOD2 function in mammalian organisms was confirmed by disruption of the SOD2 gene, which turns out to be lethal for mice due to neurodegeneration and damage to the heart (Lebovitz et al., 1996). These suggest that SOD2 plays an especially important role in the detoxification of ROS and superoxide anion radicals.

At present, a heterozygous *Sod2* knockout mouse, whose Sod2 activity is decreased by 55% in the liver, has been developed (Van Remmen et al., 1999). However, mouse is much smaller than rat, which is the most frequently used experimental animal for pharmacological and toxicological studies in the drug development process because of its body weight and ease of sampling blood or urine. A standard technique of gene knockout in rat has not been established yet. Recently, recombinant adenovirus methods are being developed and used for the purpose of gene delivery (Akai et al., 2007; Yoshikawa et al., 2009). Furthermore, a small interfering RNA strategy, which has been proven to be more specific and efficient than the full-length antisense cDNA strategy, has been established (Meister and Tuschl, 2004). In a previous study, we constructed a recombinant adenovirus expressing SOD2-short hairpin RNA (AdSOD2-shRNA) that could knockdown rat SOD2 mRNA efficiently (Yoshikawa et al., 2009). In that report, a cell model with SOD2-knockdown and CYP3A4-overexpression was constructed using AdSOD2-shRNA and AdCYP3A4, and SOD2 activity was decreased by 50% with high CYP3A4 activity 3 days after infection.

* Corresponding author. Tel.: +81 76 234 4407; fax: +81 76 234 4407.
E-mail address: tyokoi@kenroku.kanazawa-u.ac.jp (T. Yokoi).

0300-483X/$ – see front matter © 2009 Elsevier Ireland Ltd. All rights reserved.
doi:10.1016/j.tox.2009.07.017

Treatment with various drugs known to induce hepatotoxicity in this cell model demonstrated a decrease in the cell viability and an increase in the production of superoxide (Yoshikawa et al., 2009). In the present study, we established the SOD2-knockdown rat model to evaluate the drug-induced hepatotoxicity with high sensitivity.

2. Materials and methods

2.1. Materials

Acetaminophen (APAP) and glutathione (GSH) were obtained from Wako Pure Chemical Industries (Osaka, Japan). ReverTra Ace (Moloney Murine Leukemia Virus Reverse Transcriptase RNaseH Minus) was from Toyobo (Tokyo, Japan). The Adenovirus Expression Vector kit (Dual Version), RNAiso, random hexamer and SYBR Premix Ex Taq were obtained from Takara (Osaka, Japan). The QuickTiter Adenovirus Titer Immunoassay kit and protein carbonyl kit were obtained from Cell Biolabs (Tokyo, Japan). Lipofectamine 2000 was obtained from Invitrogen (Grand Island, NY). The GeneSilencer shRNA Vector kit was obtained from Gene Therapy Systems (San Diego, CA). Dulbecco's modified Eagle's medium was obtained from Nissui Pharmaceutical (Tokyo, Japan). All primers and oligonucleotides for shRNA were commercially synthesized at Hokkaido System Sciences (Sapporo, Japan). Lipid peroxidation measurement kit was obtained from BIOMOL (Philadelphia, USA). Other chemicals were of analytical or the highest grade commercially available.

2.2. Animals

Male Fisher 344 rats (7 weeks old, 130–150 g) were obtained from SLC Japan (Hamamatsu, Japan). Animals were housed in a controlled environment (temperature 25 ± 1 °C, humidity 50 ± 10%, and 12 h light/12 h dark cycle) in the institutional animal facility with access to food and water *ad libitum*. Animals were acclimatized for a week before use for the experiments. Animal maintenance and treatment were conducted in accordance with the National Institutes of Health Guide for Animal Welfare of Japan, as approved by the Institutional Animal Care and Use Committee of Kanazawa University, Japan.

2.3. Design of short hairpin RNA

Rat SOD2 (Gene Bank™, accession code NM_017051 Gene bank) knockdown was achieved by RNA interference using the adenovirus vector-based short hairpin RNA (shRNA) approach as previously described (Yoshikawa et al., 2009). As a negative control, the oligonucleotide sequences of the shRNA target for luciferase from a GeneSilencer shRNA Vector kit were used.

2.4. Recombinant adenovirus

We generated the recombinant adenovirus vector expressing SOD2-shRNA (AdSOD2-shRNA) as previously described (Yoshikawa et al., 2009). In brief, pGSU6-GFP plasmids were recombined into the pAxcwit using the cosmid-terminal protein complex method according to the manufacturer's instructions. The recombinant adenovirus was isolated and propagated into the 293 cells. Then, an adenovirus containing shRNA of SOD2 was constructed. As a negative control, the oligonucleotide sequences of the shRNA target for luciferase from a GeneSilencer shRNA Vector kit were used (AdLuc-shRNA). The titer was determined by a QuickTiter Adenovirus Titer Immunoassay kit. The titers of AdSOD2-shRNA and AdLuc-shRNA were 6.0×10^9 pfu/mL and 1.0×10^{10} pfu/mL, respectively.

2.5. Real-time reverse transcription (RT)-PCR analysis

RNA from the hepatic cells was isolated using RNAiso. Rat SOD2 and glyceraldehyde-3-phosphate dehydrogenase (GAPDH) were quantified by real-time RT-PCR. The primer sequences used in this study were as follows: rat SOD2, 5′-GAGGCTATCAAGCGTGACTTTGG-3′ and 5′-AAGCGTGCTCCCACACATCAATC-3′; rat GAPDH, 5′-GTTACCAGGGCTGCCTTCTC-3′ and 5′-GGGTTTCCCGTTGATGACC-3′. For the reverse transcription process, total RNA (2 μg) and 150 ng of random hexamer were mixed and incubated at 70 °C for 10 min. RNA solution was added to a reaction mixture containing 100 units of ReverTra Ace, reaction buffer, and 0.5 mM dNTPs in a final volume of 40 μL. The reaction mixture was incubated at 30 °C for 10 min, 42 °C for 1 h, and heated at 98 °C for 10 min to inactivate the enzyme. The real-time RT-PCR was performed using the Smart Cycler (Cepheid, Sunnyvale, CA). The PCR mixture contained 1 μL of template cDNA, SYBR Premix Ex Taq solution, and 10 pmol of sense and antisense primers. The PCR condition for GAPDH and SOD2 were as follows: after an initial denaturation at 95 °C for 30 s, the amplification was performed by denaturation at 94 °C for 4 s, annealing and extension at 64 °C for 20 s for 45 cycles. Amplified products were monitored directly by measuring the increase of the dye intensity of the SYBR Green I (Molecular Probes, Eugene, OR) that binds to double strand DNA amplified by PCR.

2.6. Western blot analysis

In the SOD2, HO-1 or sulfotransferase (SULT) 1 protein measurement, 10 μg of denatured mitochondrial (SOD2) or cytosol (HO-1 and SULT1) protein were loaded per lane, separated on 15% (SOD2 and HO-1) or 7.5% (SULT1) SDS-polyacrylamide gels and transferred onto polyvinylidene difluoride (PVDF) membrane (Immobilon-P; Millipore). These specific proteins were detected by rabbit anti-human SOD2 polyclonal antibody, cross-reacting to rat SOD2 (sc-30080; Santa Cruz Biotechnology, Santa Cruz, CA), goat anti-human HO-1 polyclonal antibody, cross-reacting to rat HO-1 (sc-1796; Santa Cruz Biotechnology), and rabbit anti-human SULT1 polyclonal antibody, cross-reacting to rat SULT1 (sc-32928; Santa Cruz Biotechnology, Santa Cruz, CA) at a dilution of 1:200. The protein bands were developed by biotinylated second antibody-peroxidase reaction. The quantitative analysis of protein expression was performed using ImageQuant TL Image Analysis software (Amersham Biosciences).

2.7. SOD2 activity

The enzyme activity of SOD2 was measured in 1 μg of protein using a kit (Cayman Chemical, MI, USA). The method utilizes tetrazolium salt to quantify superoxide radicals generated by xanthine oxidase and hypoxanthine. The standard curve was generated using a quality controlled SOD standard included with the kit. SOD2 activity was determined by performing the assay in the presence of potassium cyanide to inhibit SOD1, and thus measuring the residual SOD2 activity.

2.8. GSH level

Livers (100 mg) were homogenized with ice-cold 5% sulfosalicylic acid and centrifuged at 8000 × *g* at 4 °C for 10 min. The GSH concentration in the supernatant was measured as described previously (Tietze, 1969).

2.9. Adenovirus infection and APAP administration in rats

Seven days after single intravenous injection of AdSOD2-shRNA or AdLuc-shRNA at 2.0×10^{11} pfu/body, the rats were orally administered APAP suspended in 0.5% carboxymethylcellulose (0, 300, 1000 mg/kg body weight). Blood samples were collected at 0, 1, 2, 3, and 12 h after the APAP treatment. Twenty-four hours after the administration of APAP, serum samples were collected for assessment of the transaminase levels and for APAP metabolite analysis. The liver was fixed in buffered neutral 10% formalin. The fixed samples were embedded in paraffin and sectioned at a thickness of 2 μm and stained with hematoxylin-eosin for microscopic examination. Rat liver cytosol and microsomes were prepared as described previously (Tabata et al., 2004). In all experiments, the rats were not treated by fasting prior to the APAP treatment or sacrifice.

2.10. Determination of plasma concentrations of APAP and its metabolites

The plasma concentrations of APAP and its metabolites were measured using high performance liquid chromatography (HPLC) as follows. Plasma (50 μL) was mixed with an equivalent aliquot of acetonitrile containing 200 pmol *m*-aminophenol as an internal standard. After extraction and centrifugation, the resulting supernatant was evaporated under nitrogen. The residue was diluted with the mobile phase (2% methanol–50 mM sodium acetate) before being injected into HPLC. APAP and its metabolites, APAP-glucuronide, APAP-sulfate, and APAP-mercapturate, were separated in a Mightysil RP-18 column (4.6 × 150 mm; 5 μm; Kanto Chemical, Tokyo, Japan). The retention times of APAP, APAP-glucuronide, APAP-sulfate, APAP-mercapturate, and *m*-aminophenol were 7.60, 2.75, 5.00, 10.50, and 4.20 min, respectively. APAP and the metabolites, eluted with the mobile phase at a flow rate of 1.0 mL/min, were monitored at 248 nm.

2.11. Protein carbonyl measurements

The protein carbonyl was measured in 1 μg of protein using a kit. In brief, protein samples were added to the 96 well Protein Binding Plate, and incubated at 37 °C for 3 h. After rinsed with PBS, dinitrophenylhydrorazine (DNPH) working solution was added, and incubated for 45 min at room temperature in the dark. After rinsed with PBS/ethanol (1:1, v/v), blocking solution was added, and incubated for 1 h. After rinsed with wash buffer, anti-DNP antibody was added, and incubated for 1 h. After rinsed with wash buffer, secondary antibody was added, and incubated for 1 h. After rinsed with wash buffer, substrate buffer was added, and incubated for 10 min, and then absorbance at 405 nm was measured.

2.12. Lipid peroxidation measurement

The lipid peroxidation was measured in 10 mg of protein using a kit. In brief, for each reaction, 10 μL of probucol and 640 μL of diluted R1 reagent (1:3 of methanol:N-methyl-2-phenylindole) were added, and mixed with 150 μL of 12 M HCl. Each reaction was incubated at 45 °C for 60 min and centrifuged at 10,000 × *g* for 10 min. The supernatant was taken and used to measure malondialdehyde (MDA) formation at 586 nm. MDA data were normalized versus the protein concentration.

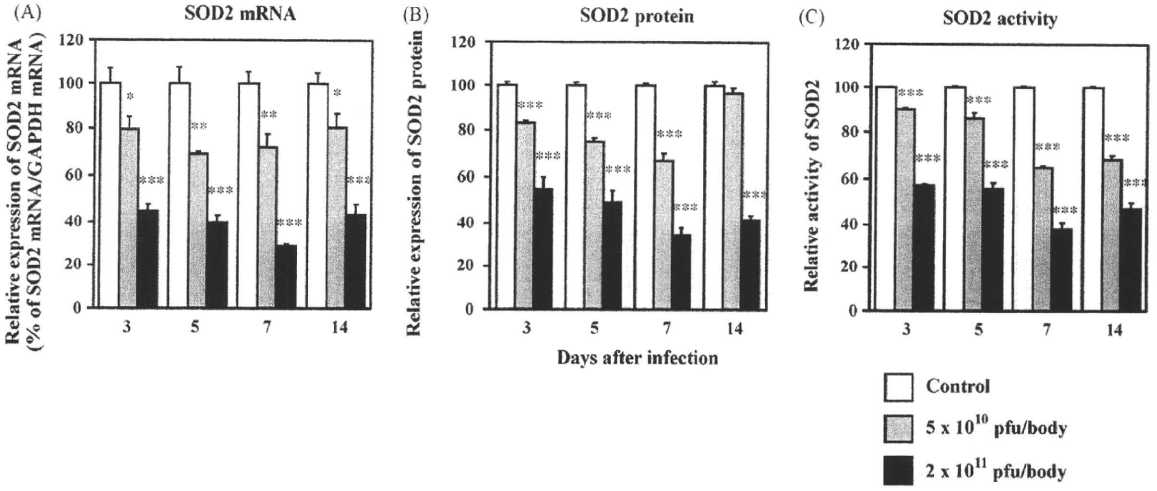

Fig. 1. Effects of adenovirus infection on hepatic SOD2 mRNA (A), protein (B), and activity (C). SOD2 mRNA (A), protein (B), and enzyme activity (C) were determined in rats infected with AdLuc-shRNA (control, 2.0×10^{11} pfu/body or AdSOD2-shRNA (5.0×10^{10} pfu/body and 2.0×10^{11} pfu/body). SOD2 protein was quantified by immunoblotting as described in Section 2. The control SOD2 enzyme activity was 12.85 ± 0.06 (U/mg protein). Data are mean ± SD ($n = 3$). $^{*}P < 0.05$, $^{**}P < 0.01$, and $^{***}P < 0.001$ compared with AdLuc-shRNA infected rats.

2.13. Statistical analysis

Statistical analyses were performed with a GraphPad Instat version 2.0 computer program (GraphPad Software, San Diego, CA) by Student *t*-test. A value of $P < 0.05$ was considered statistically significant.

3. Results

3.1. Effects of adenovirus infection on hepatic SOD2

To investigate the most efficient condition of AdSOD2-shRNA infection, Fisher-344 rats were infected with AdSOD2-shRNA at 5.0×10^{10} or 2.0×10^{11} pfu/body for 3, 5, 7, and 14 days (Fig. 1). SOD2 mRNA, protein expression, and enzyme activity began to decrease 3 days after infection, and 72%, 65%, and 61% decreases were achieved 7 days after infection in the 2.0×10^{11} pfu/body infected group, respectively. Fourteen days after infection of AdSOD2-shRNA, SOD2 mRNA, protein expression, and enzyme activity had recovered a little. These results suggested that 7 days infection would be the most efficient condition for knocking down SOD2. In addition, serum AST and ALT were not increased in any group (Supplementary Fig. 1). These results suggested that 7 days infection at 2.0×10^{11} pfu/body would be an appropriate condition for AdSOD2-shRNA infection.

3.2. Hepatotoxic effect of APAP in adenovirus-infected rats

To determine whether APAP-induced hepatotoxicity was potentiated by the suppression of hepatic SOD2, rats were tail vein-injected once with 2.0×10^{11} pfu/body AdSOD2-shRNA or AdLuc-shRNA. After 7 days, APAP was orally administered without previous fasting treatment. The serum AST and ALT levels are shown in Fig. 2A. Twenty-four hours after APAP administration, the 300 mg/kg treated groups did not demonstrate hepatotoxicity. In contrast, the AdSOD2-shRNA infected rats treated with 1000 mg/kg APAP demonstrated a significant increase of AST (114.25 ± 40.91 U/L) and ALT (51.79 ± 16.11 U/L) compared with AdLuc-shRNA infected rats. The AdLuc-shRNA rats administered 1000 mg/kg APAP did not demonstrate hepatotoxicity. The results of the histological examination in 1000 mg/kg APAP-administered rats are shown in Fig. 2B. Remarkable hepatic necrosis, especially around the central vein, and lymphocyte infiltrations were observed in AdSOD2-shRNA infected rats given 1000 mg/kg APAP, consistent with the elevation of AST and ALT. There were no histological changes in the other groups.

3.3. Changes of the plasma concentrations of APAP and its metabolites in adenovirus infected rats

Changes in the plasma concentration of APAP and its metabolites are shown in Fig. 3. For APAP and APAP-sulfate, the maximum plasma concentration was observed 1 h after APAP administration. In the AdSOD2-shRNA infected group, the time to peak concentration of APAP-glucuronide was earlier than that of the AdLuc-shRNA infected group. On the other hand, APAP-sulfate, a major detoxification product in rats generated directly from APAP, was decreased. For APAP-mercapturate, the maximum plasma concentration was observed 3 h after APAP administration in rats infected with AdSOD2-shRNA, and was significantly decreased compared with the AdLuc-shRNA infected group.

3.4. Change of expression of HO-1 protein and GSH concentration in APAP-administered rats infected with AdSOD2-shRNA

To investigate the mechanism of APAP-induced hepatotoxicity in AdSOD2-shRNA infected rats, HO-1 protein, known to be induced by oxidative stress, was measured. Superoxide itself is not able to be measured *in vivo*, thus HO-1 protein was measured as an alternative method to evaluate APAP-induced oxidative stress. The HO-1 protein band was observed only in AdSOD2-shRNA infected rats given 1000 mg/kg APAP (Fig. 4A), suggesting that APAP-induced hepatotoxicity was caused by oxidative stress. The GSH concentrations in AdSOD2-shRNA infected rats were significantly increased compared with the AdLuc-shRNA infected control rats (Fig. 4B). In contrast, the GSH concentrations in AdSOD2-shRNA infected rats given 1000 mg/kg APAP were significantly decreased compared with the AdLuc-shRNA infected rats (Fig. 4B).

3.5. Change of protein carbonyl and lipid peroxidation in APAP-administered rats infected with AdSOD2-shRNA

HO-1 was known to be induced by oxidative stress, but also induced by hypoxia. Thus, we measured protein carbonyl and lipid peroxidation in mitochondria and serum to reveal that APAP-induced hepatotoxicity in SOD2 knockdown rats was caused by

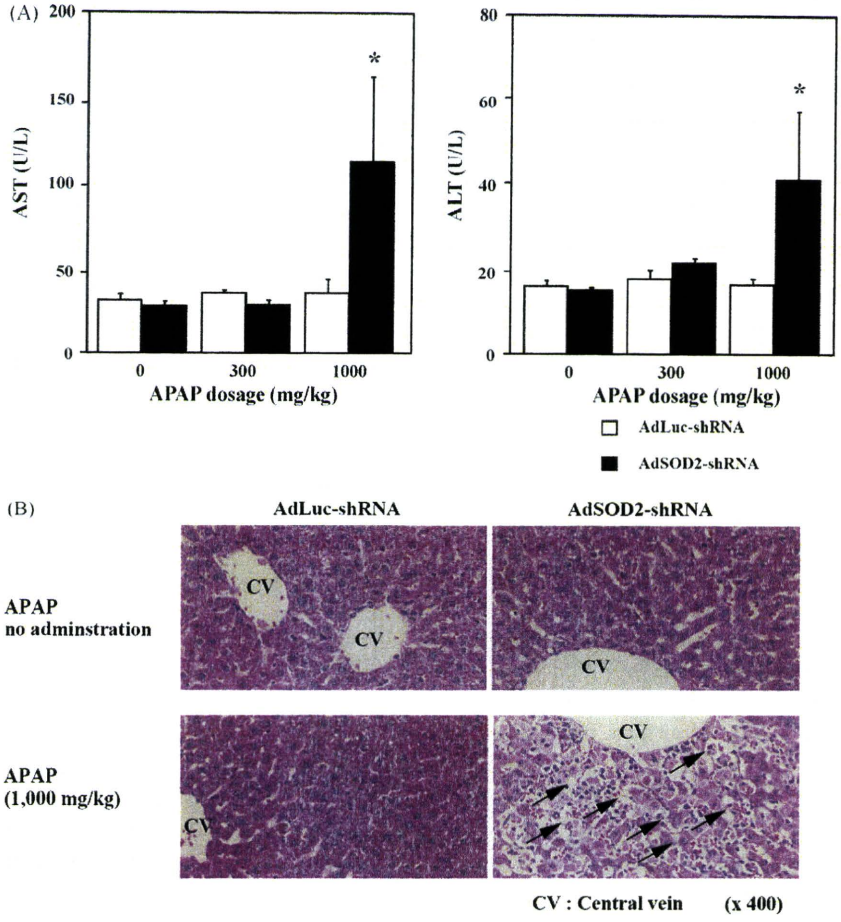

Fig. 2. Hepatotoxic effect of APAP in adenovirus-infected rats. APAP was orally administered without previous fasting. After 24 h, serum AST and ALT were measured (A). Hematoxylin-eosin staining was performed in sections of rat liver. Hepatic necrosis and lymphocyte infiltrations indicated by arrows were observed only in AdSOD2-shRNA infected rats given 1000 mg/kg APAP (B). Data are mean ± SD ($n = 5$). *$P < 0.05$ compared with AdLuc-shRNA infected rats.

oxidative stress more clearly. In both mitochondria and serum, protein carbonyl and lipid peroxidation concentrations in AdSOD2-shRNA infected rats given 1000 mg/kg APAP were significantly increased compared with the AdLuc-shRNA infected rats (Fig. 5), indicating that APAP-induced hepatotoxicity was caused by oxidative stress.

4. Discussion

In our previous study, a cell model with SOD2-knockdown and CYP3A4-overexpression was constructed using an adenovirus expressing SOD2-short hairpin RNA (AdSOD2-shRNA) and AdCYP3A4, which decreased SOD2 activity by 50% 3 days after infection with high CYP3A4 activity (Yoshikawa et al., 2009). Treatment with various drugs known to induce hepatotoxicity to this cell model demonstrated decreases in the cell viability and increases in the production of superoxide. In the present study, the SOD2 knockdown rat model was established using AdSOD2-shRNA, which decreased the SOD2 activity by 60% 7 days after infection (Fig. 1). In addition, acetaminophen (APAP)-induced hepatotoxicity was demonstrated in AdSOD2-shRNA infected rats (Fig. 2).

We successfully produced a SOD2-knockdown rat model by means of adenovirus-mediated RNA interference technology in order to detect drug-induced hepatotoxicity with high sensitivity. A previous report described that over 2.0×10^{11} pfu/body infection of an adenovirus caused adenovirus derived hepatotoxicity (Akai et al., 2007). There were no differences in AST and ALT between PBS-injected rats (AST: 31.98 ± 3.12, ALT: 16.20 ± 1.12) and adenovirus-infected rats. Therefore, we infected AdLuc-shRNA or AdSOD2-shRNA at 2.0×10^{11} pfu/body, which resulted in no hepatotoxicity. In AdSOD2-shRNA infected rats, SOD2 activity was decreased by 60% in rat liver. This decrease in the level of SOD2 is a little greater than that in heterozygous *Sod2* knockout mice (55% decrease). Therefore, we determined that a single injection of AdSOD2-shRNA (2.0×10^{11} pfu/body) was the proper condition for testing the drug-induced hepatotoxicity in this study.

In previous APAP-induced hepatotoxicity studies, in most cases rats were fasted for a half or 1 day before drug administration (Merrick et al., 2006; Kim et al., 2006; Pessayre et al., 1980). In the present study, in order to clarify the involvement of SOD2 knockdown, the rats were not fasted throughout the experiment. Previous reports demonstrated that fasting caused an approximately 50% decrease of GSH in liver. Moreover, the CYP2E1 activity is significantly increased (8- to 9-fold) by fasting (Hu et al., 1995; Jaeschke and Wendel, 1985). APAP is metabolized to *N*-acetyl-*p*-benzo-quinone imine, mainly by CYP2E1, and thus fasting would cause an overestimation of APAP-induced hepatotoxicity. As an *in vivo* hepatotoxicity screening system, a single oral administration dose of APAP at 300 and 1000 mg/kg to normal rats in a fasting condition was reported by a Pfizer group (Kikkawa et al., 2006), and there was no increase of ALT and AST at 300 mg/kg at 24 h after p.o. administration, although there was a potent increase of ALT (209.0 ± 252.3) and AST (573.3 ± 490.1) at 1000 mg/kg in normal rats. The same single oral administration of APAP (1000 mg/kg) in a

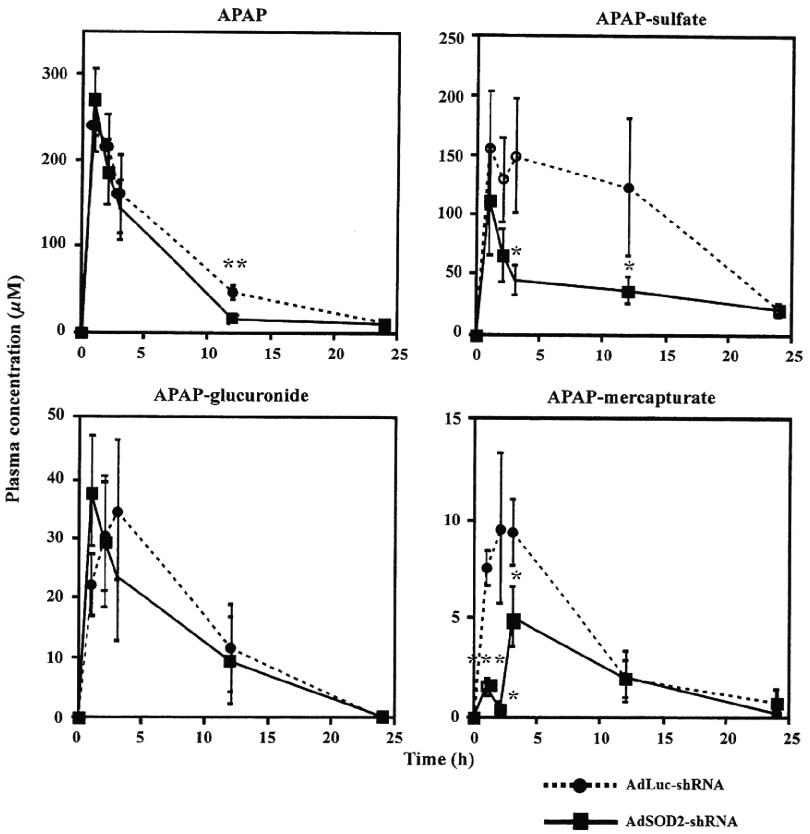

Fig. 3. Changes of the plasma concentrations of APAP and its metabolites in rats infected with the adenovirus. Rats were administered APAP (1000 mg/kg, p.o.). Data are mean ± SD ($n = 5$). $^{*}P < 0.05$, $^{**}P < 0.01$, and $^{***}P < 0.001$ compared with AdLuc-shRNA infected rats given 1000 mg/kg APAP.

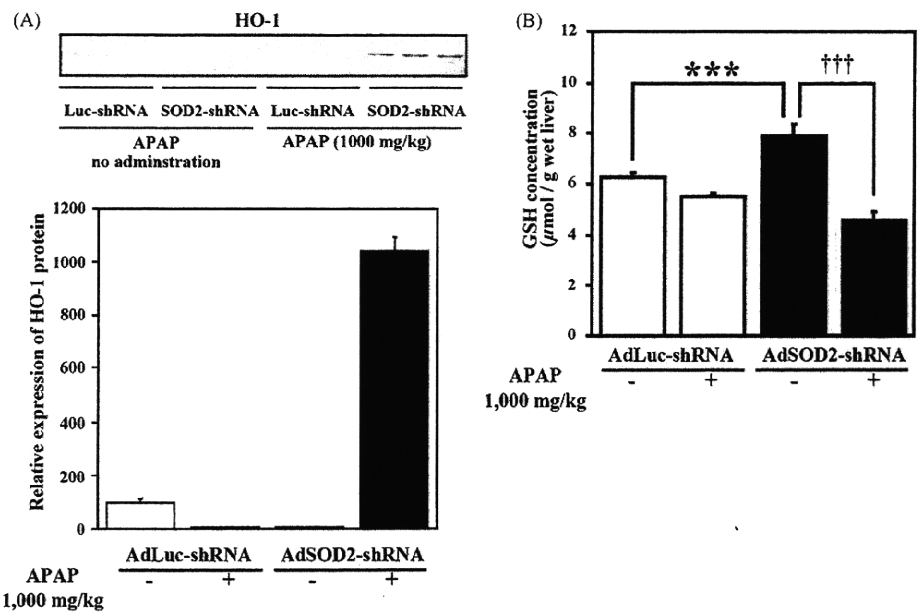

Fig. 4. Changes of expression of hepatic HO-1 protein (A) and glutathione concentration (B). HO-1 protein was detected by immunoblotting as described in Section 2 (A). In the GSH concentration measurement, rat liver was excised at 24 h after administration of saline or APAP (B). $^{***}P < 0.001$ compared with AdLuc-shRNA infected rats given saline, and $^{\dagger\dagger\dagger}P < 0.001$ compared with AdSOD2-shRNA infected rats given saline.

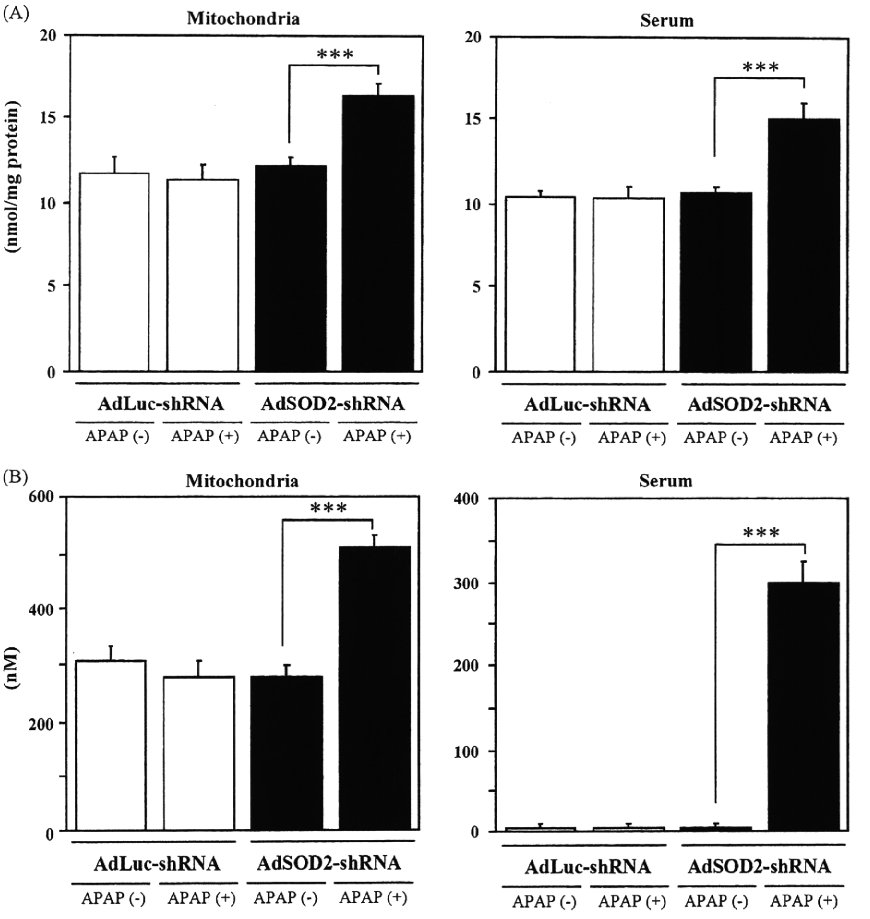

Fig. 5. Changes of protein carbonyl (A) and lipid peroxidation (B). Rats were administered APAP (1000 mg/kg, p.o.). Protein carbonyl (A) and lipid peroxidation (B) in mitochondria and serum were measured 24 h after administration of saline or APAP. Data are mean ± SD ($n = 3$). ***$P < 0.001$ compared with AdLuc-shRNA infected rats given 1000 mg/kg APAP.

fasting condition was also adopted by the National Toxicogenomics project in Japan as a screening system, and a significant increase of ALT and AST was shown at 24 h after treatment (Morishita et al., 2006). Based on these lines of considerations, we performed the experiments without fasting treatment.

Infection of AdSOD2-shRNA caused a significant decrease of APAP-sulfate in the rat plasma compared with AdLuc-shRNA infected control rats (Fig. 3), suggesting that SOD2 knockdown caused a suppression of the sulfotransferase (SULT) activity. In SOD2 knockdown rat, SULT1 expression was significantly decreased (Supplementary Fig. 2), thus the concentration of APAP-sulfate was decreased. In our previous report using adenovirus vector with short hairpin RNA against rat γ-glutamylcysteine synthetase, the concentration of APAP-sulfate was also decreased (Akai et al., 2007), thus adenovirus-mediated suppression in SULT1 protein might be occurred. However, the mechanism remains unknown. Furthermore, infection of AdSOD2-shRNA caused a significant decrease of APAP-mercapturate in the plasma. The GSH concentration was increased in AdSOD2-shRNA infected rats (Fig. 4), thus the plasma concentration of APAP-mercapturate should be increased, however, the opposite result was obtained, suggesting that the other metabolites of APAP resulted in compensatory increases, however, it was difficult to identify the whole metabolites. This result also remains to be clarified.

In the present study, APAP-induced hepatotoxicity was caused by knocking down SOD2 in rats. The mechanism of APAP-induced hepatotoxicity is very complex, and many reports have been published (McConnachie et al., 2007; Ganey et al., 2007; Gunawan et al., 2006; Lei et al., 2006). In one of these papers, APAP-induced hepatotoxicity was reported not to be occurred in *Sod1* knockout mice (Lei et al., 2006). In our study, there was no difference in SOD1 expression between AdLuc-shRNA and AdSOD2-shRNA infected group (data not shown), suggesting that SOD2 knockdown was not affected on SOD1 expression. Thus, SOD1 might be not involved in APAP-induced hepatotoxicity in SOD2 knockdown rat. Actually, it is difficult to evaluate APAP-induced hepatotoxicity only by SOD2 knockdown, as many factors are thought to be involved in the toxicity. However, it became clear that SOD2 is partly involved in APAP-induced hepatotoxicity *in vivo* in rat. In the near future, by using AdSOD2-shRNA infected rats, we will evaluate the hepatotoxicity of other drugs that induced cytotoxicity in SOD2 knockdown- and CYP3A4 overexpressing-cells in our previous report (Yoshikawa et al., 2009).

In conclusion, we firstly established SOD2-knockdown rats. This rat model could be useful as a highly sensitive drug-induced hepatotoxicity test for drug candidates in preclinical drug development.

Conflict of interest

None of the authors has any conflicts of interest related to this manuscript.

Acknowledgments

This work was supported by Health and Labor Sciences Research Grants from the Ministry of Health, Labor, and Welfare of Japan. We thank Mr. Brent Bell for reviewing the manuscript.

Appendix A. Supplementary data

Supplementary data associated with this article can be found, in the online version, at doi:10.1016/j.tox.2009.07.017.

References

Akai, S., Hosomi, H., Minami, K., Tsuneyama, K., Katoh, M., Nakajima, M., Yokoi, T., 2007. Knock down of γ-glutamylcysteine synthetase in rat causes acetaminophen-induced hepatotoxicity. J. Biol. Chem. 282, 23996–24003.

Boelsterli, U.A., Lim, P.L., 2006. Mitochondrial abnormalities—a link to idiosyncratic drug hepatotoxicity? Toxicol. Appl. Pharmacol. 220, 92–107.

Das, K.C., Guo, X.L., White, C.W., 1998. Protein kinase C delta-dependent induction of manganese superoxide dismutase gene expression by microtubule-active anticancer drugs. J. Biol. Chem. 273, 34639–34645.

Ganey, P.E., Luyendyk, J.P., Newport, S.W., Eagle, T.M., Maddox, J.F., Mackman, N., Roth, R.A., 2007. Role of the coagulation system in acetaminophen-induced hepatotoxicity in mice. Hepatology 46, 1177–1186.

Gunawan, B.K., Liu, Z.X., Han, D., Hanawa, N., Gaarde, W.A., Kaplowitz, N., 2006. c-Jun N-terminal kinase plays a major role in murine acetaminophen hepatotoxicity. Gastroenterology 131, 165–178.

Hu, Y., Ingelman-Sundberg, M., Lindros, K.O., 1995. Induction mechanisms of cytochrome P450 2E1 in liver: interplay between ethanol treatment and starvation. Biochem. Pharmacol. 50, 155–161.

Jaeschke, H., Wendel, A., 1985. Diurnal fluctuation and pharmacological alteration of mouse organ glutathione content. Biochem. Pharmacol. 34, 1029–1033.

Kaplowitz, N., 2005. Idiosyncratic drug hepatotoxicity. Nat. Rev. Drug Discov. 4, 489–499.

Kikkawa, R., Fujikawa, M., Yamamoto, T., Hamada, Y., Yamada, H., Horii, I., 2006. In vivo hepatotoxicity study of rats in comparison with in vitro hepatotoxicity screening system. J. Toxicol. Sci. 31, 23–34.

Kim, Y.W., Ki, S.H., Lee, J.R., Lee, S.J., Kim, C.W., Kim, S.C., Kim, S.G., 2006. Liquiritigenin, an aglycone of liquiritin in Glycyrrhizae radix, prevents acute liver injuries in rats induced by acetaminophen with or without buthionine sulfoximine. Chem. Biol. Interact. 161, 125–138.

Lebovitz, R.M., Zhang, H., Vogel, H., Cartwright Jr., J., Dionne, L., Lu, N., Huang, S., Matzuk, M.M., 1996. Neurodegeneration, myocardial injury, and perinatal death in mitochondrial superoxide dismutase-deficient mice. Proc. Natl. Acad. Sci. U.S.A. 93, 9782–9787.

Lei, X.G., Zhu, J.H., McClung, J.P., Aregullin, M., Roneker, C.A., 2006. Mice deficient in Cu,Zn-superoxide dismutase are resistant to acetaminophen toxicity. Biochem. J. 399, 455–461.

McConnachie, L.A., Mohar, I., Hudson, F.N., Ware, C.B., Ladiges, W.C., Fernandez, C., Chatterton-Kirchmeier, S., White, C.C., Pierce, R.H., Kavanagh, T.J., 2007. Glutamate cysteine ligase modifier subunit deficiency and gender as determinants of acetaminophen-induced hepatotoxicity in mice. Toxicol. Sci. 99, 628–636.

Meister, G., Tuschl, T., 2004. Mechanisms of gene silencing by double-stranded RNA. Nature 431, 343–349.

Merrick, B.A., Bruno, M.E., Madenspacher, J.H., Wetmore, B.A., Foley, J., Pieper, R., Zhao, M., Makusky, A.J., McGrath, A.M., Zhou, J.X., Taylor, J., Tomer, K.B., 2006. Alterations in the rat serum proteome during liver injury from acetaminophen exposure. J. Pharmacol. Exp. Ther. 318, 792–802.

Morishita, K., Mizukawa, Y., Kasahara, T., Okuyama, M., Takashima, K., Toritsuka, N., Miyagishima, T., Nagao, T., Urushidani, T., 2006. Gene expression profile in liver of differing ages of rats after single oral administration of acetaminophen. J. Toxicol. Sci. 31, 491–507.

Pessayre, D., Wandscheer, J.C., Cobert, B., Level, R., Degott, C., Batt, A.M., Martin, N., Benhamou, J.P., 1980. Additive effects of inducers and fasting on acetaminophen hepatotoxicity. Biochem. Pharmacol. 29, 2219–2223.

Tabata, T., Katoh, M., Tokudome, S., Hosakawa, M., Chiba, K., Nakajima, M., Yokoi, T., 2004. Bioactivation of capecitabine in human liver: involvement of the cytosolic enzyme on 5′-deoxy-5-fluorocytidine formation. Drug Metab. Dispos. 32, 762–767.

Tietze, F., 1969. Enzymic method for quantitative determination of nanogram amounts of total and oxidized glutathione: applications to mammalian blood and other tissues. Anal. Biochem. 27, 502–522.

Van Remmen, H., Salvador, C., Yang, H., Huang, T.T., Epstein, C.J., Richardson, A., 1999. Characterization of the antioxidant status of the heterozygous manganese superoxide dismutase knockout mouse. Arch. Biochem. Biophys. 363, 91–97.

Visner, G.A., Dougall, W.C., Wilson, J.M., Burr, I.A., Nick, H.S., 1990. Regulation of manganese superoxide dismutase by lipopolysaccharide, interleukin-1, and tumor necrosis factor. Role in the acute inflammatory response. J. Biol. Chem. 265, 2856–2864.

Yoshikawa, Y., Hosomi, H., Fukami, T., Nakajima, M., Yokoi, T., 2009. Establishment of knockdown of superoxide dismutase 2 and expression of CYP3A4 cell system to evaluate drug-induced cytotoxicity. Toxicol. In Vitro, 1179–1187.

Zelko, I.N., Mariani, T.J., Folz, R.J., 2002. Superoxide dismutase multigene family: a comparison of the CuZn-SOD (SOD1), Mn-SOD (SOD2), and EC-SOD (SOD3) gene structures, evolution, and expression. Free Radic. Biol. Med. 33, 337–349.

TOXICOLOGICAL SCIENCES 111(2), 302–310 (2009)
doi:10.1093/toxsci/kfp165
Advance Access publication July 24, 2009

Halothane-Induced Liver Injury is Mediated by Interleukin-17 in Mice

Eisuke Kobayashi,* Masanori Kobayashi,* Koichi Tsuneyama,† Tatsuki Fukami,* Miki Nakajima,* and Tsuyoshi Yokoi*,[1]

*Drug Metabolism and Toxicology, Faculty of Pharmaceutical Sciences, Kanazawa University, Kakuma-machi, Kanazawa 920-1192, Japan; and †Department of Diagnostic Pathology, Graduate School of Medicine and Pharmaceutical Science for Research, University of Toyama, Sugitani 930-0194, Toyama, Japan

Received May 23, 2009; accepted July 21, 2009

Drug-induced liver injury is a major problem in drug development and clinical drug therapy. In most cases the mechanisms are still unknown, thus, it is difficult to predict or prevent these reactions. It has been known that halothane, an inhaled anesthetic, induces liver injury. To investigate the mechanisms of halothane-induced liver injury, we used a recently established mouse model of liver injury. The expression of transcription factors and cytokines specific for Th1 and Th2 (helper T cells), respectively, were compared between BALB/c and C57BL/6 mice. The mRNA expression ratios of mouse T-bet(a Th1-specific transcription factor)/GATA-binding protein (GATA-3, a Th2-specific transcription factor) and interferon γ/interleukin (IL)-10 were lower in BALB/c mice compared with C57BL/6 mice, suggesting that a typical Th1 or Th2-dominant response could not be distinguished in halothane-induced liver injury. We observed increases of the plasma IL-17 level and hepatic macrophage inflammatory protein 2 expression in halothane-administrated BALB/c mice, as well as neutrophil infiltration. Neutralization of IL-17 suppressed the hepatotoxic effect of halothane. Administration of recombinant IL-17 (1 μg per mouse, single ip) to the halothane-treated mice resulted in a remarkable increase of alanine and aspartate aminotransferases. In conclusion, we demonstrated that IL-17 is involved in the halothane-induced liver injury.

Key Words: **cytokine; MIP-2; neutrophils; helper T cells; prostaglandin E_1.**

Drug-induced liver injury is the most frequent reason for the withdrawal of an approved drug from the market and for failures in drug development in pharmaceutical companies. Because of significant adverse drug reactions associated with hepatotoxicity, several drugs have been removed from the pharmaceutical market, including bromfenac, ebrotidine, and troglitazone (Holt and Ju, 2006). In most cases, the mechanisms of the hepatotoxicity are unknown and predictive experimental animal models are lacking.

Halothane, an inhaled anesthetic, causes asymptomatic increases of plasma transaminases in approximately 20% of patients and life-threatening fulminant hepatitis is induced in a small percentage of patients (Ray and Drummond, 1991). Halothane is metabolized to trifluoroacetyl radicals by cytochrome P450 2E1 and covalent binding to target macromolecules (Eliasson *et al.*, 1998). Although trifluoroacetylated-protein in the liver was believed to cause the liver injury, interstrain, and intrastrain differences in metabolism were not correlated with susceptibility in guinea pigs, suggesting that the inherent ability of metabolizing halothane cannot completely account for the mechanism of halothane-induced liver injury (Farrell *et al.*, 1996; Lind *et al.*, 1989).

Recently, a new animal model of halothane-induced liver injury was established which demonstrated the existence of strain differences between BALB/c and C57BL/6 mice (You *et al.*, 2006). However, no significant difference in either the patterns or levels of hepatic trifluoroacetylated-protein adducts formed in these two strains was observed.

Helper T cells (Th cells) are an important regulator of acquired immunity. Th cells are subdivided into Th1, Th2, and Th17 subsets by their unique production of cytokines and characteristic transcription factors (Kidd, 2003; Zhu and Paul, 2008). Th1 and Th2 direct different immune response pathway (Kidd, 2003). Th1 responses drive cellular immunity to kill intracellular pathogens and overactivation of Th1 cells induces some autoimmune diseases. On the other hand, Th2 responses drive humoral immunity and cause allergic inflammatory diseases including asthma (Zhu and Paul, 2008). C57BL/6 and BALB/c mice develop predominantly Th1 and Th2 responses, respectively (Knight *et al.*, 2007; Mizuhara *et al.*, 1998; Tanaka *et al.*, 1996). Mouse T box expressed in T cells (T-bet) and GATA-binding protein (GATA-3) are two major T helper–specific transcription factors that regulate the expression of Th1 or Th2 cytokine genes and play a crucial role in T-helper cell differentiation. Interferon-γ (IFN-γ) is a major cytokine of Th1 cells, whereas, interleukin-10 (IL-10) is a cytokine mainly synthesized by Th2 cells that inhibits IFN-γ expression in Th1 cells (Fiorentino *et al.*, 1989).

Th17 is a newly defined Th-cell subset which mainly produces IL-17 and plays critical roles in the protection against microbial challenges and the induction of autoimmune diseases. IL-17 can induce many inflammatory cytokines and

[1] To whom all correspondence should be addressed at Drug Metabolism and Toxicology, Faculty of Pharmaceutical Sciences, Graduate School of Medical Science, Kanazawa University, Kakuma-machi, Kanazawa 920-1192, Japan. Fax: +81-76-234-4407. E-mail: tyokoi@kenroku.kanazawa-u.ac.jp.

TABLE 1
Sequences of Primers and Annealing Temperatures Used for Real-Time RT-PCR Analyses

Target	Primer	Sequence	Annealing temperature (°C)
T-bet	FP	5′-CAA GTG GGT GCA GTG TGG AAA G-3′	68
	RP	5′-TGG AGA GAC TGC AGG ACG ATC-3′	
GATA-3	FP	5′-GGA GGA CTT CCC CAA GAG CA-3′	62
	RP	5′-CAT GCT GGA AGG GTG GTG A-3′	
IFN-γ	FP	5′-GGC CAT CAG CAA CAT AAG C-3′	68
	RP	5′-TGG ACC ACT CGG ATG AGC TCA-3′	
IL-10	FP	5′-TGA AGA CCC TCA GGA TGC GG-3′	66
	RP	5′-AGA GCT CTG TCT AGG TCC TGG-3′	
TNF-α	FP	5′-TGT CTC AGC CTC TTC TCA TTC C-3′	66
	RP	5′-TGA GGG TCT GGG CCA TAG AAC-3′	
MIP-2	FP	5′-AAG TTT GCC TTG ACC CTG AAG-3′	64
	RP	5′-ATC AGG TAC GAT CCA GGC TTC-3′	
β-Actin	FP	5′-ACG GCC AGG TCA TCA CTA TTG G-3′	68
	RP	5′-CTA GGA GCC AGA GCA GTA ATC TC-3′	

Note. FP, forward primer; RP, reverse primer.

chemokines, and thus has an important role in neutrophil infiltration and activation. Th17 cytokines secreted by T cells are suppressed by Th-2-dominant cytokines (Gu *et al.*, 2008) suggesting some involvement of IL-17.

Liver inflammation mediated by neutrophils has been demonstrated in some experimental animal models showing ethanol-, acetaminophen-, and α-naphthyl-isothiocyanate–induced liver inflammation and ischemia-reperfusion liver injury (Ramaiah and Jaeschke, 2007). Although, the role of neutrophils in the pathogenesis of halothane-induced liver injury was demonstrated previously (You *et al.*, 2006), Th cell involvement, which has been implicated as critical in some autoimmune diseases (Zhu and Paul, 2008), remains unknown. In this study, we investigated whether Th cells play an important role in halothane-induced liver injury. First, the expressions of transcription factors and cytokines specific for Th1 and Th2, respectively, were compared between susceptible and tolerant mice strains. Second, to investigate IL-17 involvement, the plasma IL-17 level was measured, and neutralization and administration of recombinant IL-17 were performed.

MATERIALS AND METHODS

Chemicals. Halothane was purchased from Sigma (St Louis, MO). Transaminase CII-test Wako was from Wako Pure Chemical Industries (Osaka, Japan). RNAiso was from Nippon Gene (Tokyo, Japan). ReverTra Ace was from Toyobo (Tokyo, Japan). Random hexamer and SYBR Premix Ex Taq were from Takara (Osaka, Japan). All primers were commercially synthesized at Hokkaido System Sciences (Sapporo, Japan). Prostaglandin E_1 (PGE_1) was purchased from Nippon Chemiphar (Tokyo, Japan). Monoclonal anti-mouse IL-17 antibody, rat IgG2a isotype and recombinant mouse IL-17 were from R&D Systems (Abingdon, UK). A Ready-SET-GO! Mouse Interleukin-17A (IL-17A) enzyme-linked immunosorbent assay (ELISA) kit was from eBioscience (San Diego, CA). Other chemicals were of analytical or the highest grade commercially available.

Halothane administration. Female BALB/cCrSlc mice and C57BL/6JJmsSlc (6–7 weeks old, 15–21 g) were obtained from SLC Japan (Hamamatsu, Japan). Animals were housed in a controlled environment (temperature 25 ± 1°C, humidity 50 ± 10%, and 12-h light/12-h dark cycle) in the institutional animal facility with access to food and water *ad libitum*. Animals were acclimatized before use for the experiments. Mice were administered ip halothane (600 μmol per mouse, dissolved in 2 ml of olive oil) in a nonfasting condition. At 3, 6, 12, and 24 h after halothane administration, the animals were sacrificed and the blood and the liver were collected. For measurement of the plasma IL-17 level, mice were sacrificed at 1, 3, 6, 9, 12, and 24 h after the halothane administration. A portion of each excised liver was fixed in 10% formalin neutral buffer solution and used for immunohistochemical staining. The degree of liver injury was assessed by hematoxylin-eosin (H&E) staining and plasma aspartate aminotransferase (AST) and alanine aminotransferase (ALT) levels were measured by Transaminase CII-test Wako according to the manufacturer's instructions. The neutrophil infiltration was assessed by immunostaining for the myeloperoxidase (MPO). Animal maintenance and treatment were conducted in accordance with the National Institutes of Health Guide for Animal Welfare of Japan, as approved by the Institutional Animal Care and Use Committee of Kanazawa University, Japan.

Real-time RT-PCR. RNA from the mouse liver was isolated using RNAiso according to the manufacturer's instructions. T-bet, GATA-3, IFN-γ, IL-10, tumor necrosis factor α (TNF-α), macrophage inflammatory ptrotein-2 (MIP-2), and β-actin were quantified by real-time RT-PCR. The primer sequences used in this study are shown in Table 1. For the RT-process, total RNA (10 μg) and 150 ng random hexamer were mixed and incubated at 70°C for 10 min. RNA solution was added to a reaction mixture containing 100 units of ReverTra Ace (Reverse transcriptase, TOYOBO, Tokyo, Japan), reaction buffer and 0.5mM deoxy-nucleotide triphosphates in a final volume of 40 μl. The reaction mixture was incubated at 30°C for 10 min, 42°C for 1 h, and heated at 98°C for 10 min to inactivate the enzyme. The real-time RT-PCR was performed using the Mx3000P (Stratagene, La Jolla, CA). The PCR mixture contained 1 or 2 μl of template cDNA, SYBR Premix Ex Taq solution, and 8 pmol of forward and reverse primers. Amplified products were monitored directly by measuring the increase of the dye intensity of the SYBR Green I (Molecular Probes, Eugene, OR) that binds to the double-strand DNA amplified by PCR.

Administration of anti-mouse IL-17 antibody or recombinant mouse IL-17. Nine hours after halothane administration, mice were administered anti-mouse IL-17 antibody intraperitoneally (100 μg of anti-mouse IL-17 antibody in 0.5 ml of sterile phosphate buffered saline [PBS]) in nonfasting condition. As a control, rat IgG2a was administered (100 μg of rat IgG2a in 0.5 ml of sterile PBS). One hour before halothane administration, recombinant

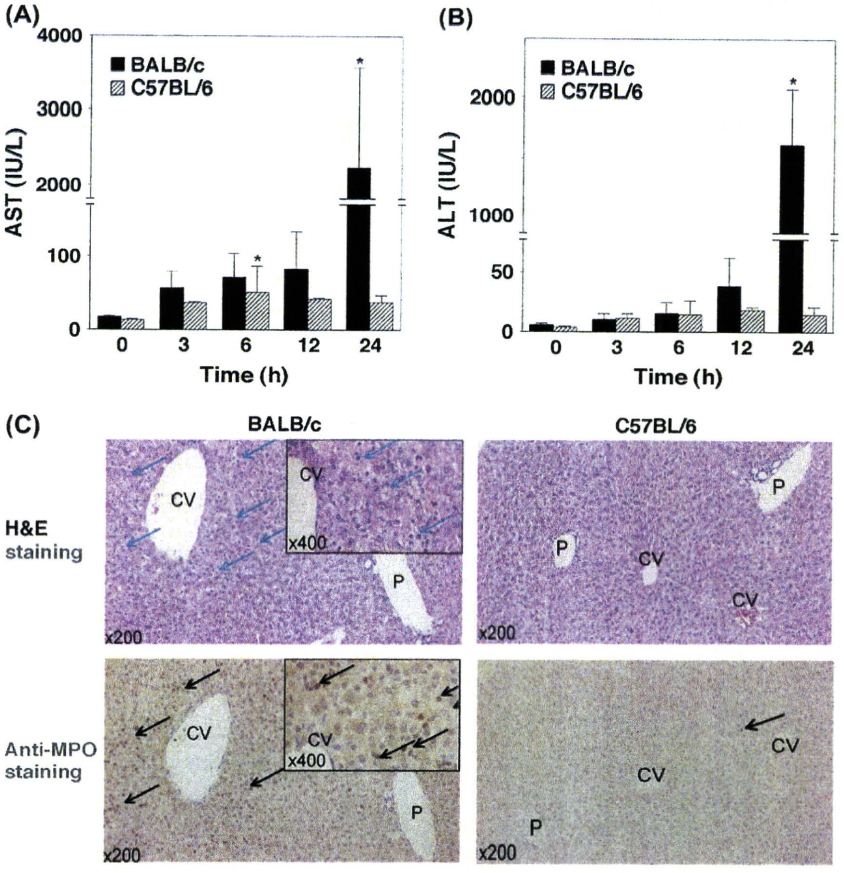

FIG. 1. Change of plasma AST and ALT levels and histological presentation of liver injury in halothane-administrated mice. Mice were administrated halothane (600 μmol per mouse, ip), and plasma for the AST (A) and ALT (B) assay were collected 3, 6, 12, and 24 h after administration. The data are means ± SD of 5–14 mice. Significantly different from control group (*$p < 0.05$). Liver specimens were sampled 24 h after halothane administration (C). Then, liver tissue sections were stained with H&E or immunostained with anti-MPO antibody. Arrows indicated necrotic cells and MPO-positive cells. CV, central vein; P, portal vein.

mouse IL-17 was intraperitoneally administered (1 μg of recombinant IL-17 in 0.2 ml of sterile PBS containing 0.5% BSA) in nonfasting condition. As a control, vehicle was administered.

Treatment of PGE_1. Six, 9, or 12 h after halothane administration, mice were treated with PGE_1 intraperitoneally (50 μg/20 g bw, dissolved in 500 μl of sterile saline) in nonfasting condition. As a control, vehicle was administered.

Measurement of plasma IL-17 level. The plasma IL-17 level was measured by ELISA using a Ready-SET-GO! Mouse IL-17A kit from eBioscience (San Diego, CA) according to the manufacturer's instructions.

Statistical analysis. Data are presented as mean ± SD. Statistical analyses between multiple groups were performed using one-way ANOVA with a *post hoc* test of significance between individual groups. Comparisons between two groups were carried out using two-tailed Student's *t*-test. $p < 0.05$ was considered statistically significant.

RESULTS

Increase of Plasma AST and ALT Levels in Halothane-Administrated BALB/c Mice

Female BALB/c and C57BL/6 mice were administered halothane at a dose of 600 μmol per mouse. Halothane administration resulted in a slight increase of the plasma AST and ALT levels in C57BL/6 mice, whereas a marked increase of the AST and ALT levels was observed 24 h after the administration in BALB/c mice (Figs. 1A and 1B).

Infiltration of Neutrophils in BALB/c Mouse Liver after Halothane Administration

Liver histology demonstrated that C57BL/6 mice had normal liver architecture, whereas focal necrosis in the centrilobular areas was observed in BALB/c mouse liver (Fig. 1C). In addition, immunohistochemical analysis with anti-MPO antibody demonstrated that a number of MPO-positive cells had infiltrated in BALB/c mouse liver at 24 h after halothane administration.

Expression of Transcription Factors and Cytokines Genes in Halothane-Administered Mouse Liver

To investigate the involvement of Th cells in the induction of halothane hepatotoxicity, hepatic mRNA of T-bet, GATA-3, IFN-γ, and IL-10 were measured by real-time RT-PCR. It was

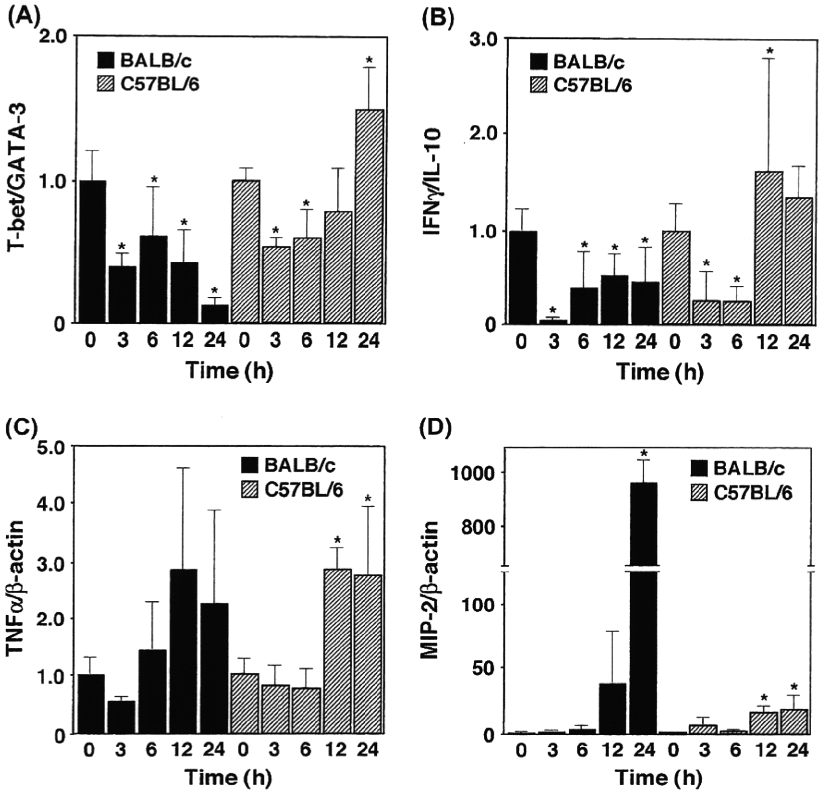

FIG. 2. Changes of hepatic mRNA expression in halothane-administrated mice. Mice were administrated halothane (600 μmol per mouse, ip). After 3, 6, 12, and 24 h, relative expression of hepatic mRNA was measured for T-bet/GATA-3 (A), IFN-γ/IL-10 (B), TNF-α/β-actin (C), and MIP-2/β-actin (D) by real-time RT-PCR. The data are means ± SD of three mice. Significantly different from control group (*$p < 0.05$).

suggested that the mRNA expression ratio of T-bet/GATA-3 and IFN-γ/IL-10 rather than the expression of either transcription factor alone reflected more closely in the Th1/Th2 cytokine balance (Chakir *et al.*, 2003). The T-bet/GATA-3 mRNA expression ratio was decreased at all time points after the administration of halothane in BALB/c mice, whereas the ratio was low at around 3–6 h and relatively high at 12–24 h in C57BL/6 mice (Fig. 2A). The IFN-γ/IL-10 mRNA expression ratio became similar to the T-bet/GATA-3 mRNA expression ratio (Fig. 2B). The T-bet/GATA-3 and IFN-γ/IL-10 mRNA expression ratio was lower in BALB/c mice compared with C57BL/6 mice. From these results, a typical Th1- or Th2-dominant response could not be distinguished. However, the mRNA expression of GATA-3 and IL-10 was relatively increased in BALB/c mice compared with C57BL/6 mice.

Measurement of Proinflammatory Cytokine and CXC Chemokine

To investigate whether the changes in liver injury and neutrophil infiltration observed in halothane-administered BALB/c mice resulted from increases of proinflammatory cytokine and CXC chemokine, we measured hepatic TNF-α and MIP-2 mRNA expression. TNF-α was slightly increased in both strains (Fig. 2C). At 12 and 24 h after halothane administration in BALB/c mice, a high SD value was observed. Thus, from these results, no conclusion about the involvement of TNF-α could be drawn (Fig. 2C). MIP-2 was markedly increased in BALB/c mice 24 h after halothane administration (Fig. 2D). These results suggested that MIP-2 may be involved in the neutrophil infiltration.

Time-Dependent Changes of Plasma Il-17 Level in Halothane Administered Mice, and Effects of Anti-IL-17 Antibody Administration

IL-17 is a cytokine produced by the newly defined Th cell subset Th17 which has inflammatory effects. To investigate whether IL-17 was involved in the infiltration of neutrophils in halothane-induced liver injury, we conducted a set of neutralization studies. Before the neutralization study, time-dependent changes of the plasma IL-17 level were measured. Mice were administered ip halothane (600 μmol per mouse) in nonfasting condition. The IL-17 level was significantly increased only 24 h after the halothane administration (Fig. 3A). ALT and AST were significantly increased in BALB/c mice as

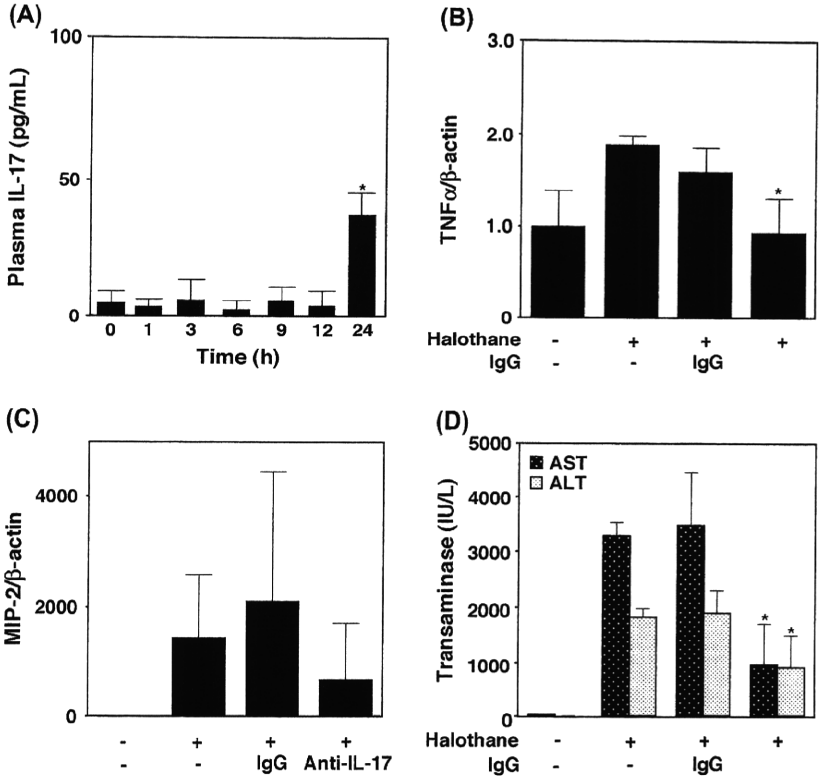

FIG. 3. Effect of anti-mouse IL-17 antibody administration on hepatic mRNA expression and plasma AST and ALT levels in halothane-administrated BALB/c mice. Mice were administrated halothane (600 μmol per mouse, ip). Plasma IL-17 level was measured 1, 3, 6, 9, 12, and 24 h after the halothane administration (A). Some mice were administrated with anti-mouse IL-17 antibody (100 μg per mouse, ip) or with rat IgG2a 9 h after the halothane administration. Twenty-four hours after halothane administration, relative expression of hepatic mRNA was measured for TNF-α/β-actin (B), and MIP-2/β-actin (C) by real-time RT-PCR. Plasma for the AST and ALT assay were collected 24 h after the halothane administration (D). The data are means ± SD of three to five mice. Significantly different from halothane- plus IgG2a-administrated group (*$p < 0.05$).

demonstrated in Figures 1A and 1B. In the neutralization study, the ip administration of a specific anti-mouse IL-17 antibody 9 h after halothane administration reduced hepatic TNF-α mRNA increases and plasma AST and ALT levels at 24 h after halothane administration (Figs. 3B and 3D). The expression of MIP-2 mRNA showed a tendency to decrease by the anti-IL-17 antibody administration (Fig. 3C). These inhibitory effects were not observed by the administration of rat IgG2a. As a preliminary study, we investigated to find the appropriate time for the administration of anti-IL-17 antibody at 3, 6, and 9 h after the halothane administration, as well as one hour before the halothane administration. As a result, the 9-h group showed the lowest expression levels of hepatic TNF-α, MIP-2 mRNA, AST, and ALT (data not shown). These results indicated that the halothane-induced liver injury was significantly suppressed by the administration of anti-IL-17 antibody.

Exacerbation of Hepatotoxic Effect by Recombinant IL-17 Administration

To further investigate whether IL-17 was involved in the halothane-induced liver injury, we performed a recombinant mouse IL-17 administration study. The ip administration of recombinant IL-17 at 1 h before the halothane administration caused remarkable increases of plasma aminotransferases at 12 and 24 h after halothane administration (Fig. 4A). To clarify the exacerbation of the hepatotoxic effect by the administration of recombinant IL-17, the dose of halothane was decreased to one half (300 μmol per mouse, ip) in this experiment. This dose of halothane (300 μmol per mouse) caused almost no increase of the plasma ALT and AST levels (data not shown). In the recombinant IL-17 and halothane-administered mice, the plasma IL-17 level remained relatively high (Fig. 4B). In the recombinant IL-17 and no-halothane–administered mice, the plasma IL-17 level was decreased to the same level as the nontreated mice indicating that the recombinant IL-17 had decreased completely at 24 h after the halothane adiministration.

Effect of Prostaglandin E_1 Treatment on Plasma IL-17 Level

Prostaglandins E series (PGEs) are known to protect against drug-induced and immune-mediated liver injury by down-regulating the production of inflammatory cytokines. It was reported that the Th2-like response of liver T cells might

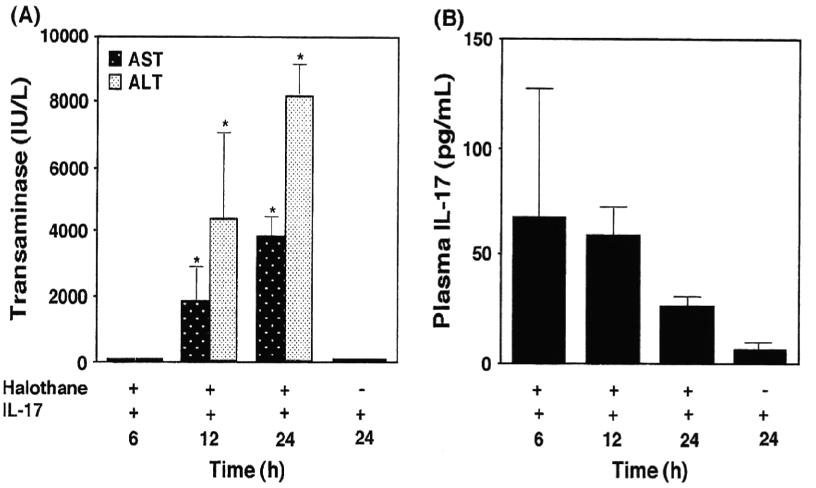

FIG. 4. Effect of recombinant mouse IL-17 administration on plasma AST, ALT, and IL-17 levels in halothane-administrated BALB/c mice. Mice were administrated halothane (300 μmol per mouse, ip). One hour before the halothane administration, recombinant mouse IL-17 (1 μg per mouse, ip) was administered. After 6, 12, and 24 h, plasma AST, ALT, and IL-17 levels were measured. The data are means ± SD of three to five mice. Significantly different from 6-h group (*$p < 0.05$).

involved in the mechanism whereby PGE_1 protects against liver injury (Mokuno *et al.*, 1999). PGE_1 inhibited the functions of neutrophils (Talpain *et al.*, 1995). However, the effect of PGE_1 on the plasma IL-17 level was not elucidated. To investigate the effect of PGE_1 on the plasma IL-17 level, PGE_1 conjugated by α-cyclodextrin was intraperitoneally administered to BALB/c mice and the plasma IL-17 level was measured by using ELISA. The plasma IL-17 level was increased in BALB/c mice 24 h after halothane administration and significantly inhibited by PGE_1 administration, whereas no change was observed in C57BL/6 mice (Fig. 5). The increase of the plasma IL-17 level in BALB/c mice suggested that this cytokine may account for strain differences in the susceptibility to halothane-induced liver injury.

Inhibition of Hepatic TNF-α and MIP-2 mRNA Expression in PGE_1-Treated Mice

We next investigated whether the hepatic expression of proinflammatory cytokines and CXC chemokines are changed in PGE_1-treated mice. The hepatic MIP-2 mRNA expression 24 h after halothane administration was significantly inhibited by treatment with PGE_1, whereas the TNF-α increase was not affected by PGE_1 (Figs. 6A and 6B). These results suggested that PGE_1 could inhibit the increase of MIP-2 expression via IL-17 signaling.

Protective Effect of PGE_1 Treatment Against Halothane-Induced Liver Injury

To investigate the protective effect of PGE_1 on the halothane-induced liver injury, we treated BALB/c mice with PGE_1, and measured the plasma AST and ALT levels 24 h after halothane administration. PGE_1 treatment significantly inhibited the increase of the plasma AST and ALT levels by halothane in BALB/c mice 9 h after halothane administration (Fig. 6C). Therefore, PGE_1 demonstrated a protective effect against halothane-induced liver injury in BALB/c mice.

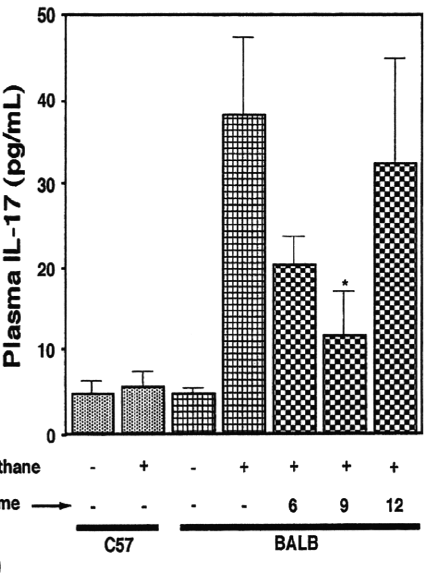

FIG. 5. Effect of PGE_1 treatment on plasma IL-17 level in halothane-administrated mice. Mice were administrated halothane (600 μmol per mouse, ip). BALB/c mice were treated with PGE_1 (50 μg/20 g bw, ip) 6, 9, or 12 h after the halothane administration. Twenty-four hours after the halothane administration, plasma IL-17 level was measured using ELISA. The data are means ± SD of three to five mice. Significantly different from halothane-administrated plus PGE_1-nontreated group (*$p < 0.05$).

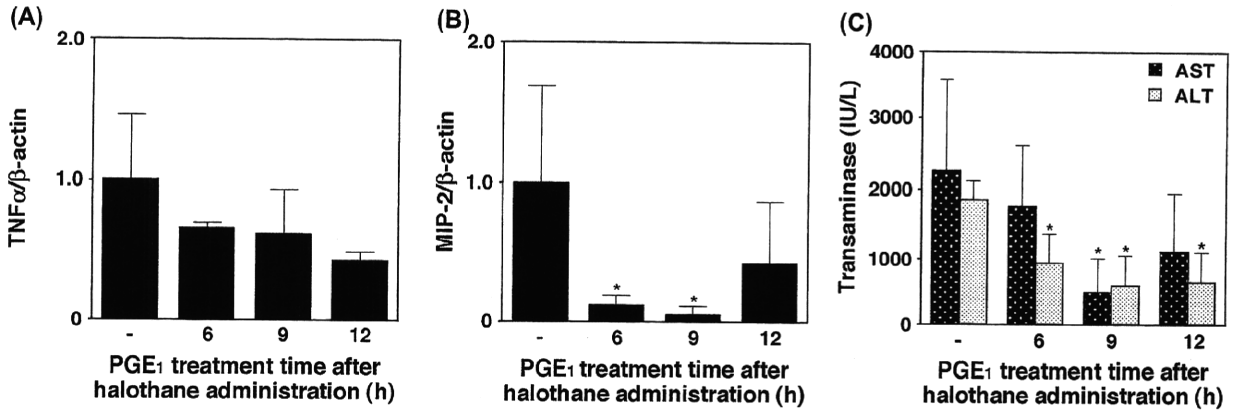

FIG. 6. Effect of PGE_1 treatment on hepatic mRNA expression in halothane-administrated BALB/c mice. Mice were administrated halothane (600 μmol per mouse, ip). Mice were treated with PGE_1 (50 μg/20g bw, ip) 6, 9, or 12 h after the halothane administration. Twenty-four hours after the halothane administration, hepatic mRNA expression was measured for TNF-α/β-actin (A), and MIP-2/β-actin (B) by real-time RT-PCR. Plasma for the AST and ALT assay were collected 24 h after the halothane administration (C). The data are means ± SD of three to four mice. Significantly different from halothane administrated plus PGE_1-nontreated group ($*p < 0.05$).

DISCUSSION

In this study, we investigated whether Th2-dominant BALB/c mice were more susceptible to halothane-induced liver injury than Th1-dominant C57BL/6 mice and whether MPO-positive cells had infiltrated in the hepatic centrilobular areas of halothane-administered BALB/c mice (Fig. 1). These results were consistent with those of previous studies in guinea pig (Lunam *et al.*, 1989) and mouse models (You *et al.*, 2006).

Previous studies have shown that T-bet and GATA-3 were Th1- and Th2-specific transcription factor, respectively (Szabo *et al.*, 2000; Zhang *et al.*, 1997). IFN-γ is a typical Th1 cytokine, and some studies suggested its involvement in T-cell–mediated liver injury and autoimmune disease (Kidd, 2003; Siebler *et al.*, 2003). IL-10 inhibits inflammatory cytokines (Glimcher and Murphy, 2000). Firstly, we investigated the relationship between halothane-induced liver injury and Th-cell–related factors. The hepatic T-bet/GATA-3 and IFN-γ/IL-10 mRNA expression ratios were decreased in susceptible BALB/c mice compared with C57BL/6 mice (Fig. 2). It was suggested that the mRNA expression ratio of T-bet/GATA-3 rather than the expression of either transcription factor alone reflected more closely the Th1/Th2 cytokine balance (Chakir *et al.*, 2003). The present observation suggested that the Th2 response would be driven in halothane-administered BALB/c mice and that a Th1/Th2 disbalance may be involved in halothane-induced liver injury as is the case for acetaminophen, lipopolysaccharide (LPS), and concanavalin A (Masubuchi *et al.*, 2008; Mizuhara *et al.*, 1998; Tanaka *et al.*, 1996). Although the increase of the hepatic mRNA expression of the proinflammatory mediator TNF-α was observed by halothane administration in both strains, we found that CXC chemokine MIP-2 mRNA expression was markedly increased only in BALB/c mice (Fig. 2). These results suggested that MIP-2 might be involved in halothane-induced liver injury.

IL-17, which is produced mainly by a specific subset of Th cells named Th17, stimulates the production of CXC chemokines (such as MIP-2 and keratinocyte-derived chemokine) and plays an important role in neutrophil activity (Zhu and Paul, 2008). Since the discovery of Th17, some immune-mediated diseases previously recognized as mediated by overactivation of the Th1-dominant response such as experimental autoimmune encephalomyelitis, collagen-induced arthritis, and inflammatory bowel disease, have now been suggested to be induced, at least in part, by Th17 cells (Zhu and Paul, 2008). It was demonstrated that IL-10 negatively regulates the expression of Th17 cytokines by both macrophages and T cells (Gu *et al.*, 2008). These lines of evidence prompted us to investigate the involvement of IL-17 in halothane-induced liver injury.

In the present study, we demonstrated that the plasma IL-17 level was increased by halothane administration in BALB/c mice, but not in C57BL/6 mice (Fig. 4), and neutralization of IL-17 significantly inhibited the increase of the plasma AST and ALT levels (Fig. 3C). In addition, the neutralization study demonstrated that the increase of MIP-2 expression in halothane-administered BALB/c mice was mediated by IL-17 (Fig. 3B). The administration of recombinant IL-17 caused a remarkable increase of the plasma AST and ALT levels (Fig. 4A) resulting in exacerbation of the hepatotoxic effect. From these lines of evidence, it is suggested that IL-17 is involved in the pathogenesis or exacerbation of halothane-induced liver injury. To the best of our knowledge, this is the first study demonstrating the involvement of IL-17 in drug-induced liver injury. The involvement of IL-17 in hepatotoxicity will be investigated in detail in the near future.

PGEs are known to protect against drug-induced liver injury or immune-mediated liver injury by downregulating the production of inflammatory cytokines. It was reported that the Th2-like response of liver T cells might be involved in the mechanism whereby PGE_1 protects against liver injury (Mokuno *et al.*, 1999). It has been demonstrated that PGE_1 inhibited superoxide production by neutrophils (Talpain *et al.*, 1995) and had a protective effect against carbon tetrachloride- and LPS-induced liver injury (Akamatsu *et al.*, 2001; Kayano *et al.*, 1995; Lindemann *et al.*, 2003; Mokuno *et al.*, 1999). However, no study has demonstrated the effect of PGE_1 on the plasma IL-17 level. These lines of reported data prompted us to investigate the effect of PGE_1 on the IL-17–related signaling in halothane-induced liver injury. In this study, the increased plasma IL-17 level, hepatic MIP-2 mRNA expression, and plasma AST and ALT levels in halothane-administrated BALB/c mice were inhibited by PGE_1 treatment (Figs. 5 and 6). Although many mechanisms of the protective effects of PGE_1 in liver injury have been elucidated, in the present study we found that inhibiting the IL-17 signal pathway could be one of the protective mechanisms of PGE_1 in halothane-induced liver injury.

A previous study suggested that p38 mitogen-activated protein kinase (MAPK) and NF-κB signaling pathway were activated in halothane-administered IL-10 deficient C57BL/6 mice (Feng *et al.*, 2009). In addition, the involvement of IL-17 in the p38 MAPK and nuclear factor kappa B (NF-κB)–signaling pathway was reported in human cardiac fibroblasts (Cortez *et al.*, 2007), and it was demonstrated that IL-10 negatively regulates the expression of Th17 cytokines and retinoid orphan receptor (RORγt) by both macrophages and T cells (Gu *et al.*, 2008). These reports supported the result of the present neutralization study.

Although the mechanism of drug-induced liver injury is still unclear due to the lack of animal models, LPS-treated rodents become sensitive to human hepatotoxic drugs, such as ranitidine, diclofenac, chlorpromazine, and trovafloxacin (Luyendyk *et al.*, 2003; Shaw *et al.*, 2009). LPS administration increased IL-17 in rodents (Ferretti *et al.*, 2003), but the involvement of IL-17 in the drug-induced liver injury in LPS-administered rodents was never reported. In addition to these LPS-drug models, mice deficient in IL-2– and suppressor of cytokine signaling (SOCS3-), which are negative regulators of the Th17-dominant response, were suggested to be useful for predicting human hepatotoxic drug candidates (Chen *et al.*, 2006; Romagnani, 2008). However, hepatic cytochrome P450s were markedly changed in a manner that was interleukin-concentration dependent (Siewert *et al.*, 2000). Especially, CYP2E1, the major enzyme of halothane metabolism, was down- or upregulated by various inflammatory cytokines (Hakkola *et al.*, 2003; Lagadic-Gossmann *et al.*, 2000), and Phase II detoxification abilities were lowered by interleukin (Romero *et al.*, 2002). Therefore, changes of the expression of drug metabolizing enzymes should be carefully pre-evaluated using IL-17 knockout mice.

The discovery of the Th17 T cell subset was a breakthrough that came from experimental autoimmune mice models (Romagnani, 2008). Although IL-17 has been recognized recently, a number of studies suggesting that IL-17 plays a critical function in autoimmune responses and protection against microbial challenges were already reported not only in mice but also in human. The present study supported the usefulness of the plasma IL-17 level for monitoring the severity of acute hepatic injury in human (Yasumi *et al.*, 2007).

In conclusion, we firstly reported that IL-17 determined the susceptibility against halothane-induced liver injury in mice. The marked increase of CXC chemokine MIP-2 and the increase of IL-17 in halothane-administered mice were investigated. Furthermore, PGE_1 treatment lowered the plasma IL-17 level and hepatic MIP-2 expression and protected against halothane-induced liver injury in mice. The present study sheds light on the mechanisms of drug-induced liver injury.

FUNDING

Health and Labor Sciences Research Grants from the Ministry of Health, Labor, and Welfare of Japan (H20-BIO-G001).

ACKNOWLEDGMENTS

We thank Mr Brent Bell for reviewing the manuscript.

REFERENCES

Akamatsu, K., Yamasaki, Y., Nishikawa, M., Takakura, Y., and Hashida, M. (2001). Synthesis and pharmacological activity of a novel water-soluble hepatocyte-specific polymeric prodrug of prostaglandin E_1 using lactosylated poly(L-glutamic hydrazide) as a carrier. *Biochem. Pharmacol.* **62,** 1531–1536.

Chakir, H., Wang, H., Lefebvre, D. E., Webb, J., and Scott, F. W. (2003). T-bet/GATA-3 ratio as a measure of the Th1/Th2 cytokine profile in mixed cell populations: Predominant role of GATA-3. *J. Immunol. Methods* **278,** 157–169.

Chen, Z., Laurence, A., Kanno, Y., Pacher-Zavisin, M., Zhu, B. M., Tato, C., Yoshimura, A., Henninghausen, L., and O'Shea, J. J. (2006). Selective regulatory function of Socs3 in the formation of IL-17-secreting T cells. *Proc. Natl. Acad. Sci. U. S. A.* **103,** 8137–8142.

Cortez, D. M., Feldman, M. D., Mummidi, S., Valente, A. J., Steffensen, B., Vincenti, M., Barnes, J. L., and Chandrasekar, B. (2007). IL-17 stimulates MMP-1 expression in primary human cardiac fibroblasts via p38 MAPK- and ERK1/2-dependent C/EBP-, NF-κB, and AP-1 activation. *Am. J. Physiol. Heart Circ. Physiol.* **293,** H3356–H3365.

Eliasson, E., Gardner, I., Hume-Smith, H., de Waziers, I., Beaune, P., and Kenna, J. G. (1998). Interindividual variability in P450-dependent generation of neoantigens in halothane hepatitis. *Chem. Biol. Interact.* **116,** 123–141.

Farrell, G. C., Frost, L., Tapner, M., Field, J., Weltman, M., and Mahoney, J. (1996). Halothane-induced liver injury in guinea-pigs: Importance of cytochrome P450 enzyme activity and hepatic blood flow. *J. Gastroenterol. Hepatol.* **11,** 594–601.

Feng, D., Wang, Y., Xu, Y., Luo, Q., Lan, B., and Xu, L. (2009). Interleukin 10 deficiency exacerbates halothane induced liver injury by increasing interleukin 8 expression and neutrophil infiltration. *Biochem. Pharmacol.* **77,** 277–284.

Ferretti, S., Bonneau, O., Dubois, G. R., Jones, C. E., and Trifilieff, A. (2003). IL-17, produced by lymphocytes and neutrophils, is necessary for lipopolysaccharide-induced airway neutrophilia: IL-15 as a possible trigger. *J. Immunol.* **170,** 2106–2112.

Fiorentino, D. F., Bond, M. W., and Mosmann, T. R. (1989). Two types of mouse T helper cell. IV. Th2 clone secrete a factor that inhibits cytokine production by Th1 clones. *J. Exp. Med.* **170,** 2081–2095.

Glimcher, L. H., and Murphy, K. M. (2000). Lineage commitment in the immune system: The T helper lymphocyte grows up. *Genes Dev.* **14,** 1693–1711.

Gu, Y., Yang, J., Ouyang, X., Liu, W., Li, H., Yang, J., Bromberg, J., Chen, S. H., Mayer, L., Unkeless, J. C., *et al.* (2008). Interleukin 10 suppresses Th17 cytokines secreted by macrophages and T cells. *Eur. J. Immunol.* **38,** 1807–1813.

Hakkola, J., Hu, Y., and Ingelman-Sundberg, M. (2003). Mechanisms of down-regulation of CYP2E1 expression by inflammatory cytokines in rat hepatome cell. *J. Pharmacol. Exp. Ther.* **304,** 1048–1054.

Holt, M. P., and Ju, C. (2006). Mechanisms of drug-induced liver injury. *AAPS J* **8,** E48–E54.

Kayano, K., Sakaida, I., Kubota, M., Yasunaga, M., and Okita, K. (1995). Functional differences between activated and normal rat liver macrophages: LPS uptake capacity by flow cytometric analysis in contrast with TNFα release. *Liver* **15,** 253–259.

Kidd, P. (2003). Th1/Th2 balance: The hypothesis, its limitations, and implications for health and disease. *Altern. Med. Rev.* **8,** 223–246.

Knight, B., Akhurst, B., Matthews, V. B., Ruddell, R. G., Ramm, G. A., Abraham, L. J., Olynyk, J. K., and Yeoh, G. C. (2007). Attenuated liver progenitor (oval) cell and fibrogenic responses to the choline deficient, ethionine supplemented diet in the BALB/c inbred strain of mice. *J. Hepatol.* **46,** 134–141.

Lagadic-Gossmann, D., Lerche, C., Rissel, M., Joannard, F., Galisteo, M., Guillouzo, A., and Corcos, L. (2000). The induction of the human hepatic CYP2E1 gene by interleukin 4 is transcriptional and regulated by protein kinase C. *Cell Biol. Toxicol.* **26,** 221–233.

Lind, R. C., Gandolfi, A. J., and Hall, P. D. (1989). Age and gender influence halothane-associated hepatotoxicity in strain 13 guinea pigs. *Anesthesiology* **71,** 878–884.

Lindemann, S., Gierer, C., and Darius, H. (2003). Prostacyclin inhibits adhesion of polymorphonuclear leukocytes to human vascular endothelial cells due to adhesion molecule independent regulatory mechanisms. *Basic Res. Cardiol.* **98,** 8–15.

Lunam, C. A., Hall, P. M., and Cousins, M. J. (1989). The pathology of halothane hepatotoxicity in a guinea-pig model: A comparison with human halothane hepatitis. *Br. J. Exp. Pathol.* **70,** 533–541.

Luyendyk, J. P., Maddox, J. F., Cosma, G. N., Ganey, P. E., Cockerell, G. L., and Roth, R. A. (2003). Ranitidine treatment during a modest inflammatory response precipitates idiosyncrasy-like liver injury in rats. *J. Pharmacol. Exp. Ther.* **307,** 9–16.

Masubuchi, Y., Sugiyama, S., and Horie, T. (2008). Th1/Th2 cytokine balance as a determinant of acetaminophen-induced liver injury. *Chem. Biol. Interact.* **179,** 273–279.

Mizuhara, H., Kuno, M., Seki, N., Yu, W. G., Yamaoka, M., Yamashita, M., Ogawa, T., Kaneda, K., Fujii, T., Senoh, H., *et al.* (1998). Strain difference in the induction of T-cell activation-associated, interferon gamma-dependent hepatic injury in mice. *Hepatology* **27,** 513–519.

Mokuno, Y., Takano, M., Matsuguchi, T., Nishimura, H., Washizu, J., Naiki, Y., Nimura, Y., and Yoshikai, Y. (1999). Prostaglandin E_1 protects against liver injury induced by *Escherichia coli* infection via a dominant Th2-like response of liver T cells in mice. *Hepatology* **30,** 1464–1472.

Ramaiah, S. K., and Jaeschke, H. (2007). Role of neutrophils in the pathogenesis of acute inflammatory liver injury. *Toxicol. Pathol.* **35,** 757–766.

Ray, D. C., and Drummond, G. B. (1991). Halothane hepatitis. *Br. J. Anaesthesiol.* **67,** 84–99.

Romagnani, S. (2008). Human Th17 cells. *Arthritis Res. Ther.* **10,** 206.

Romero, L., Higgins, M. A., Gilmore, J., Boudreau, K., Maslen, A., Barker, H. J., and Kirby, G. M. (2002). Down-regulation of alpha class glutathione S-transferase by interleukin-1beta in human intestinal epithelial cells (Caco-2) in culture. *Drug Metab. Dispos.* **30,** 1186–1193.

Shaw, P. J., Ditewig, A. C., Waring, J. F., Liguori, M. J., Blomme, E. A., Ganey, P. E., and Roth, R. A. (2009). Coexposure of mice to trovafloxacin and lipopolysaccharide, a model of idiosyncratic hepatotoxicity, results in a unique gene expression profile and interferon γ-dependent liver injury. *Toxicol. Sci.* **107,** 270–280.

Siebler, J., Wirtz, S., Klein, S., Protschka, M., Blessing, M., Galle, P. R., and Neurath, M. F. (2003). A key pathogenic role for the STAT1/T-bet signaling pathway in T-cell-mediated liver inflammation. *Hepatology* **38,** 1573–1580.

Siewert, E., Bort, R., Kluge, R., Heinrich, P. C., Castell, J., and Jover, R. (2000). Hepatic cytochrome P450 down-regulation during aseptic inflammation in the mouse is interleukin 6 dependent. *Hepatology* **32,** 49–55.

Szabo, S. J., Kim, S. T., Costa, G. L., Zhang, X., Fathman, C. G., and Glimcher, L. H. (2000). A novel transcription factor, T-bet, directs Th1 lineage commitment. *Cell* **100,** 655–669.

Talpain, E., Armstrong, R. A., Coleman, R. A., and Vardey, C. J. (1995). Characterization of the PGE receptor subtype mediating inhibition of superoxide production in human neutrophils. *Br. J. Pharmacol.* **114,** 1459–1465.

Tanaka, Y., Takahashi, A., Watanabe, K., Takayama, K., Yahata, T., Habu, S., and Nishimura, T. (1996). A pivotal role of IL-12 in Th1-dependent mouse liver injury. *Int. Immunol.* **8,** 569–576.

Yasumi, Y., Takikawa, Y., Endo, R., and Suzuki, K. (2007). Interleukin-17 as a new marker of severity of acute hepatic injury. *Hepatol. Res.* **37,** 248–254.

You, Q., Cheng, L., Reilly, T. P., Wegmann, D., and Ju, C. (2006). Role of neutrophils in a mouse model of halothane-induced liver injury. *Hepatology* **44,** 1421–1431.

Zhang, D. H., Cohn, L., Ray, P., Bottomly, K., and Ray, A. (1997). Transcription factor GATA-3 is differentially expressed in murine Th1 and Th2 cells and controls Th2-specific expression of the interleukin-5 gene. *J. Biol. Chem.* **272,** 21597–21603.

Zhu, J., and Paul, W. E. (2008). CD4 T cells: Fates, functions, and faults. *Blood* **112,** 1557–1569.